

AEDC-TR-68-136

**ARCHIVE COPY  
DO NOT LOAN**

*Fig 1*



# **FURTHER EXPERIMENTS ON MIXING AND BURNING OF BOUNDED COAXIAL STREAMS**

**T. H. M. Cunningham and C. E. Peters**

**ARO, Inc.**

**October 1968**

This document has been approved for public release  
and sale; its distribution is unlimited.

AEDC TECHNICAL LIBRARY



5 0720 00031 7588

**ROCKET TEST FACILITY  
ARNOLD ENGINEERING DEVELOPMENT CENTER  
AIR FORCE SYSTEMS COMMAND  
ARNOLD AIR FORCE STATION, TENNESSEE**

PROPERTY OF U. S. AIR FORCE  
AEDC LIBRARY  
F40600-69-C-0001

# ***NOTICES***

When U. S. Government drawings specifications, or other data are used for any purpose other than a definitely related Government procurement operation, the Government thereby incurs no responsibility nor any obligation whatsoever, and the fact that the Government may have formulated, furnished, or in any way supplied the said drawings, specifications, or other data, is not to be regarded by implication or otherwise, or in any manner licensing the holder or any other person or corporation, or conveying any rights or permission to manufacture, use, or sell any patented invention that may in any way be related thereto.

Qualified users may obtain copies of this report from the Defense Documentation Center.

References to named commercial products in this report are not to be considered in any sense as an endorsement of the product by the United States Air Force or the Government.

FURTHER EXPERIMENTS ON MIXING AND  
BURNING OF BOUNDED COAXIAL STREAMS

T. H. M. Cunningham and C. E. Peters  
ARO, Inc.

This document has been approved for public release  
and sale; its distribution is unlimited.

**FOREWORD**

The research presented was sponsored by the Arnold Engineering Development Center (AEDC), Air Force Systems Command (AFSC), Arnold Air Force Station, Tennessee, under Program Element 6540223F.

The results of the research were obtained by ARO, Inc., (a subsidiary of Sverdrup & Parcel and Associates, Inc.), contract operator of AEDC under Contract F40600-69-C-0001. The work was conducted under ARO Project No. RW3518 in the Research Branch of the Rocket Test Facility (RTF), and the manuscript was submitted for publication as partial results of this research effort on May 29, 1968.

This technical report has been reviewed and is approved.

Marion L. Laster  
Aerospace Engineer  
Research Division  
Directorate of Plans  
and Technology

Edward R. Feicht  
Colonel, USAF  
Director of Plans  
and Technology

**ABSTRACT**

Results of bounded mixing and burning experiments in relatively long ducts are presented. The series of experiments was part of a theoretical and experimental investigation of bounded mixing with combustion within ducts of arbitrary shape. The mixing system consisted of a fuel-rich,  $H_2-O_2$  rocket stream and a surrounding stream of room-temperature air. A conical mixing duct with cylindrical extensions was used. Twenty-six rocket firings were made in the test series. The system was operated in the "downstream choking" mode (independent of back pressure) for 19 firings and in the "back pressure dependent" mode for the remainder of the series. Stagnation pressure ratio between the two streams was varied to provide a range of data. Data presented include axial distributions of wall static pressure and radial profiles of gas composition and pitot pressure at the mixing duct exit.

## CONTENTS

	<u>Page</u>
ABSTRACT. . . . .	iii
NOMENCLATURE. . . . .	vii
I. INTRODUCTION . . . . .	1
II. EXPERIMENTAL PROGRAM	
2.1 Rocket Engine . . . . .	3
2.2 Mixing Duct . . . . .	4
2.3 Instrumentation. . . . .	4
2.4 Experimental Procedure. . . . .	6
III. RESULTS AND DISCUSSION	
3.1 Downstream Choking Experiments . . . . .	7
3.2 Back Pressure Dependent Experiments . . . . .	9
3.3 Comparison of Upstream Choking and Downstream Choking Modes . . . . .	10
IV. CONCLUDING REMARKS . . . . .	11
REFERENCES . . . . .	12

## APPENDICES

## I. ILLUSTRATIONS

Figure

1. Schematic of Air-Augmented Rocket. . . . .	15
2. Operational Modes of a Ducted Mixing System	
a. Upstream Choking Mode . . . . .	16
b. Back Pressure Dependent Mode. . . . .	17
c. Downstream Choking Mode. . . . .	18
3. Schematic of Propulsion Research Cell (R-1B) . . . . .	19
4. Rocket Engine . . . . .	20
5. Details of Water-Cooled Spark Plug. . . . .	21
6. Survey Rake	
a. Rake Geometry . . . . .	22
b. Probe Tip Details . . . . .	22
7. Mass Flow Ratio, Downstream Choking Mode . . . . .	23

<u>Figure</u>	<u>Page</u>
8. Mixing Duct Thrust, Downstream Choking Mode. . .	24
9. Duct Wall Pressure, Downstream Choking Mode	
a. Test Condition 1 . . . . .	25
b. Test Condition 2 . . . . .	26
c. Test Condition 3 . . . . .	27
d. Test Condition 4 . . . . .	28
e. Test Condition 5 . . . . .	29
f. Test Condition 6 . . . . .	30
10. Pitot Pressure at Duct Exit, Downstream Choking Mode	
a. Test Condition 2 . . . . .	31
b. Test Condition 3 . . . . .	32
c. Test Condition 4 . . . . .	33
d. Test Condition 5 . . . . .	34
e. Test Condition 6 . . . . .	35
11. Composition at Duct Exit, Downstream Choking Mode . . . . .	36
12. Duct Wall Pressure, Back Pressure Dependent Mode	
a. Test Condition 7 . . . . .	37
b. Test Condition 8 . . . . .	38
c. Test Condition 9 . . . . .	39
d. Test Condition 10 . . . . .	40
e. Test Condition 11 . . . . .	41
f. Test Condition 12 . . . . .	42
g. Test Condition 13 . . . . .	43
13. Pitot Pressure at Duct Exit, Back Pressure Dependent Mode	
a. Test Condition 8 . . . . .	44
b. Test Condition 9 . . . . .	45
c. Test Condition 10 . . . . .	46
d. Test Condition 12 . . . . .	47
e. Test Condition 13 . . . . .	48
14. Composition at Duct Exit, Downstream Choking Mode	
a. Test Condition 8 . . . . .	49
b. Test Condition 9 . . . . .	50
c. Test Condition 10 . . . . .	51
15. Comparison of Upstream Choking and Downstream Choking Mode	
a. Mass Flow Ratio . . . . .	52
b. Thrust Ratio . . . . .	53

	<u>Page</u>
II. TABLES	
I. Experimental Parameters. . . . .	54
II. Summary of Test Conditions, Downstream Choking Mode . . . . .	55
III. Summary of Test Conditions, Back Pressure Dependent Mode . . . . .	56

### NOMENCLATURE

A	Area
$c^*$	Characteristic velocity defined by Eq. (1)
D	Mixing duct diameter
$F_D$	Mixing duct thrust given by Eq. (2)
$F_j$	Rocket vacuum thrust defined by Eq. (3)
$g_c$	Constant of proportionality in Newton's second law
$L^*$	Characteristic length of rocket chamber
$L_1$	Length of conical mixing duct
$L_2$	Length of cylindrical mixing duct extension
M	Mach number
O/F	Rocket oxidizer-fuel mass ratio
p	Static pressure
$p_b$	Back pressure
$p_d$	Spray chamber pressure
$p_o$	Stagnation (or total) pressure
$p'_o$	Pitot pressure
r	Radius
$r_n$	Rocket exit radius
$T_o$	Stagnation (or total) temperature
w	Mass flow

x	Axial distance from duct inlet
$\alpha$	Nozzle divergence half-angle
$\gamma$	Ratio of specific heats
$\lambda$	Nozzle divergence correction factor, defined by Eq. (4)

**SUBSCRIPTS**

1	Mixing duct inlet
2	Exit of conical mixing duct
a	Outer inviscid stream (secondary)
av	Average of firings with nominally the same conditions
e	Exit of rocket nozzle
j	Center inviscid stream (primary)
t	Throat of nozzle
w	Mixing duct wall

## SECTION I INTRODUCTION

The phenomenon of ducted turbulent mixing of coaxial streams occurs in many engineering applications such as in propulsion systems and in jet pumps. Of particular interest here is the mixing and burning of a fuel-rich rocket exhaust jet with a surrounding annulus of air. This type of mixing which occurs in the air-augmented rocket (Refs. 1 and 2) is shown schematically in Fig. 1 (Appendix I). The overall thrust of the vehicle will be higher than the basic rocket thrust if the internal pressure forces acting on the mixing duct are larger than the combined inlet and external drag. Experimental and theoretical research on ducted mixing systems typical of the air-augmented rocket has been in progress for several years at the Rocket Test Facility (RTF) of the Arnold Engineering Development Center (Ref. 3).

When the primary (central) stream of a ducted mixing system is supersonic and the secondary (outer) stream is initially subsonic, three modes of operation are possible (Fig. 2). The major difference in these modes is the mechanism which controls the secondary stream mass flow ( $w_a$ ). The "upstream choking" mode (Fig. 2a) occurs when the central jet expands outward, causing a choke point in the secondary flow. Downstream of the choking section, the secondary flow is supersonic. This mode was termed "supersonic regime" by Fabri and Paulon (Ref. 4) in their work on supersonic air-air ejectors. The choking section occurs near the entrance of the mixing duct, and the secondary mass flow rate is primarily limited by the inviscid interaction of the two streams, with viscous effects only slightly influencing the secondary mass flow rate (Ref. 5). The experiments on ducted rocket-air mixing reported in Ref. 3 were in the upstream choking mode.

A special case of the upstream choking mode occurs when the minimum secondary flow area is at the initial section. This case was termed "saturated supersonic regime" by Fabri, and the overexpanded central jet deflects inward rather than pluming outward. Because the area of the choked secondary flow is fixed,  $w_a$  is directly proportional to  $p_{0a}$ .

The second mode of operation of a ducted mixing system is shown in Fig. 2b. In this "back pressure dependent" mode the secondary flow is subsonic throughout the duct, and the secondary flow rate is determined by matching the duct exit pressure with the relatively high back pressure. This mode was termed the "mixed regime" by Fabri.

The third mode of operation, "downstream choking," is shown in Fig. 2c. The mixing duct flow is independent of back pressure and is controlled by choking at or near the duct exit. In a cylindrical or divergent mixing duct, this mode will probably be encountered only when there is considerable heat release in the downstream mixing process. The secondary flow is subsonic throughout the duct, and the wall pressures are fairly constant. This downstream choking mode is desirable for the air-augmented rocket because the internal pressure forces are quite high compared with the upstream choking mode.

Perini, et al. (Ref. 1) showed with simplified analysis (complete mixing at duct exit, constant wall pressure) that optimum thrust performance of an air-augmented rocket is obtained when the secondary stream remains subsonic. It is doubtful whether the assumption of complete mixing at the duct exit can be realized in mixing ducts of practical length. If the ducted mixing system is operated in the downstream choking mode, however, the wall pressures can be maintained approximately constant even when the back pressure is relatively low. It would appear, therefore, that an actual ducted mixing system operated in the downstream choking mode would approach the idealized optimum air-augmented rocket of Perini, et al.

Experimental results are presented in this report for a mixing system in which the primary (central) jet is the exhaust from a fuel-rich hydrogen-oxygen ( $H_2-O_2$ ) rocket and the secondary (outer) flow is air. Relatively long mixing ducts were tested; therefore, with low back pressure the mixing system was operated in the downstream choking mode. Some results are also presented for the mixing system in the back pressure dependent mode of operation. The data presented include secondary-primary mass flow ratios, mixing duct wall pressure distributions, mixing duct thrust, and radial profiles of pitot pressure and gas composition at the duct exit plane.

The experimental results have not been compared with theory in this report. The integral mixing theory reported in Ref. 3 has been substantially improved, and a report covering the correlation of the theory with these and other experimental results is in preparation.

## SECTION II EXPERIMENTAL PROGRAM

The RTF Propulsion Research Cell (R-1B) (Fig. 3) was designed to investigate the bounded mixing and burning process. A small scale rocket was used for the primary stream, and atmospheric air supplied the secondary stream. Flow rate of the primary stream was held nearly constant for

all experiments, and the secondary flow rate was varied by throttling the atmospheric inflow. The cell was connected to the RTF Plant Exhauster System, which controlled back pressure on the mixing duct while inbleeding sufficient air to safely dilute the combustible gases. Principal dimensions and operating parameters for the cell and rocket engine are given in Table I (Appendix II).

In addition to the measurements of rocket and airstream parameters, the following information was obtained:

1. Mixing duct static pressure distribution,
2. Pitot pressure distribution across the mixing duct exit plane, and
3. Gas composition distributions across the mixing duct exit plane.

## 2.1 ROCKET ENGINE

A water-cooled, gaseous  $H_2-O_2$  rocket engine was used to generate the primary stream of hot, fuel-rich (2.5 times stoichiometric fuel) exhaust gases. A cross section of the rocket is presented in Fig. 4. A copper injector head and liner were used; the outer shell and water baffle were of stainless steel. The water baffle with integral spacers was fastened around the liner, and the assembly was inserted into the outer shell. Silicone rubber O-rings were used to seal the internal joints. The design of the O-ring joint at the nozzle exit allowed relative growth between liner and shell. The flow pattern from the fuel and oxidizer injector ports converged to a point. Hydrogen was injected from the inner ring of ports to prevent destructive oxidation of the spark plug tip. The characteristic length,  $L^*$  (chamber volume/throat area), of the rocket engine was approximately 35 in. The theoretical chamber temperature was approximately 5300°R.

The  $H_2-O_2$  propellant combination was chosen because of the relatively simple exhaust gas composition which lends itself readily to gas analysis. Gaseous propellants were chosen to achieve a high combustion efficiency; liquid-propellant rocket engines of this scale normally operate at much lower combustion efficiency than a comparable large booster engine. A rocket engine having high combustion efficiency is necessary for accurate experimental evaluation of rocket thrust augmentation configurations in which afterburning of the rocket exhaust occurs. If the rocket is inefficient, an unrealistically large amount of unburned fuel is

available for afterburning. This excessive afterburning can lead to erroneous conclusions about the performance of the augmented rocket as compared with that of the basic rocket.

The characteristic velocity ( $c^*$ ) is commonly used as a measure of combustion efficiency. The following relationship defines  $c^*$ :

$$c^* = \frac{P_{0j} A_t g_c}{w_j} \quad (1)$$

For the 26 firings discussed in this report, the experimentally determined value of  $c^*$  averaged 96.5 percent of theoretical.

A water-cooled spark plug was used to initiate combustion. A cross section of the device is shown in Fig. 5. This design provided rapid starts and proved to be extremely long lived.

## 2.2 MIXING DUCT

The experiments reported in Ref. 3 were made with a conical mixing duct (configuration A). The experiments reported herein were made with the same conical mixing duct, but the duct length was increased by installation of a cylindrical extension. Mixing duct configuration B (Table I) consisted of the conical duct with a 6-in. -long extension ( $L_2$ , Fig. 3). The cylindrical extension was 9 in. long for configuration C.

## 2.3 INSTRUMENTATION

### 2.3.1 Wall Static Pressure

Wall static pressures throughout the apparatus were measured with mercury manometers, referenced to atmosphere, and recorded photographically. Mixing duct static pressures were measured with two rows of taps 90 deg apart; the axial tap spacing was 2 in.

A vacuum check was made before and after each test to detect any leaks in the manometer system. The scales on the manometers were subdivided into 0.1-in. increments, and the resulting pressures were read with an estimated precision of  $\pm 0.05$  psi.

### 2.3.2 Airflow Rate

The secondary airflow was measured with a choked venturi (Fig. 3), having a circular arc inlet contour and a conical diffuser section. For

the range of throat Reynolds number encountered, the nozzle flow coefficient was greater than 0.99 (Ref. 6); therefore, the coefficient was assumed to be unity. The stagnation pressure of the venturi flow was measured with a mercury manometer, and the stagnation temperature was measured with an immersion-type thermocouple.

### 2.3.3 Rocket Flow Rate

The rocket flow rate was calculated by summing the propellant flow rates. The gaseous-propellant flows were measured with choked venturis having circular arc inlets and conical diffuser sections. Propellant temperatures were measured with immersion-type thermocouples, which were located just downstream from the diffuser sections to avoid disturbing the venturi inlet flows. At this location, the flows were again subsonic, and thus accurate temperature indications were ensured. The nozzle flow coefficients were again, for the range of Reynolds number encountered, greater than 0.99 (Ref. 6).

### 2.3.4 Rocket System Pressures

Rocket chamber pressure and the propellant metering nozzle inlet pressures were measured with strain-gage-type transducers and recorded on direct-inking, null-balance potentiometers. The systems were periodically calibrated against a known pressure to check for nonlinearity and for absolute level. The calibrations were checked prior to each test period by applying a fixed resistance to the system to obtain a full-scale deflection. During shakedown of the apparatus, the propellant pressures downstream from the metering nozzles were measured with similar instrumentation. These pressure measurements were discontinued after it was found that the pressure drops across the venturis were sufficient to ensure choked flow at the nozzle throats.

### 2.3.5 Temperatures

Airstream total temperature was measured with an immersion-type thermocouple and recorded on a multipoint, null-balance potentiometer.

The propellant temperatures were measured with immersion-type thermocouples and recorded on a light-beam oscillograph. The thermocouple system was calibrated by applying known voltage from a standard cell and recording the galvanometer deflection. The thermocouples were referenced to control room temperature, which was measured with a mercury bulb thermometer.

### 2.3.6 Survey Rake

The mixing duct exit plane surveys were made with a water-cooled, 13-probe rake having seven pitot pressure probes and six gas sampling probes (Fig. 6). The rake was installed with the probe tips about 0.25 in. downstream from the mixing duct exit. A complete survey of the exit plane flow was accomplished by installing the rake during different tests at various positions relative to the duct centerline. Details of the probe tip construction are shown in Fig. 6b.

The gas sampling probes were similar to those used by Rhodes, et al. (Ref. 7) in their investigation of shock-induced combustion of H<sub>2</sub>-air mixtures. A sapphire watch bearing (fused aluminum-oxide) was imbedded in the probe tip to provide an orifice capable of withstanding the high stream temperatures. The probe was designed so that the expansion of the sample flow inside the probe and the cooling effect of the inner probe walls would cause quenching of the major chemical reactions. The gas samples were taken in evacuated bottles and were later analyzed for nitrogen (N<sub>2</sub>), O<sub>2</sub>, and H<sub>2</sub> with a mass spectrograph, which had been calibrated with known samples.

The rake pitot pressures were measured with mercury manometers referenced to atmosphere. Near the duct centerline, however, the pressures were too high to be measured with the available 100-in. manometers, and dial-type bourdon-tube gages were used. These gages were graduated in 0.2-psi increments and could be read with an estimated precision of  $\pm 0.1$  psi.

## 2.4 EXPERIMENTAL PROCEDURE

With the exhaust pressure at the desired value, the desired secondary flow was set by adjusting the throttle valve upstream from the metering venturi. The rocket was then fired for a nominal duration of 30 sec. The system was allowed to stabilize for 20 sec before samples were collected and pressures were recorded.

## SECTION III RESULTS AND DISCUSSION

This presentation of data is divided into three sections. The first deals with data obtained from the downstream choking mode, and the second covers a number of tests performed in the back pressure dependent mode. The third compares the performance of ducted mixing systems operating in the upstream choking and downstream choking modes.

### 3.1 DOWNSTREAM CHOKING EXPERIMENTS

Six test conditions were run with the system operated in the downstream choking mode, and the resulting data are presented in Table II and Figs. 7 through 11. Nine firings were made in test condition 2 and six firings in test condition 3. Single firings were made in test conditions 1, 4, 5, and 6. The gas sampling-pitot pressure rake was shifted radially before each firing of conditions 2 and 3 to provide complete profiles across the duct exit. Most of the flow parameters tabulated in Table II have been discussed in Sections 2.1 and 2.3. Items that required elaboration in this section are mixing duct thrust ( $F_D$ ) and rocket vacuum thrust ( $F_j$ ). Mixing duct thrust was determined from the expression,

$$F_D = \int_{A_1}^{A_2} p_w d A_D \quad (2)$$

The integral was evaluated graphically from plots of experimental pressure distribution as a function of duct area. The rocket vacuum thrust is defined as

$$F_j = p_e A_e \lambda (1 - \gamma M_e^2) \quad (3)$$

where  $\lambda$  is the nozzle divergence correction factor given by

$$\lambda = \frac{1}{2} (1 + \cos \alpha) \quad (4)$$

$F_j$  represents the thrust of the engine in a vacuum and is a convenient reference.

#### 3.1.1 Secondary-Primary Mass Flow Ratio

The mass flow ratio ( $w_a/w_j$ ) is plotted in Fig. 7 as a function of the stagnation pressure ratio ( $p_{0a}/p_{0j}$ ). All these data were obtained with mixing duct configuration B (6-in. extension). The individual firings of test conditions 2 and 3 are plotted rather than the test condition averages.

#### 3.1.2 Mixing Duct Thrust

The mixing duct thrust ratio ( $F_D/F_j$ ) is plotted in Fig. 8 as a function of  $p_{0a}/p_{0j}$ . As in Fig. 7, the thrust ratios were obtained with mixing duct configuration B. Again, the individual firings of test conditions 2 and 3 are plotted.

#### 3.1.3 Wall Pressure Distributions

Axial distributions of the duct wall static pressure are shown in Fig. 9. The pressure distribution shown in Fig. 9a was obtained with

mixing duct C (9-in. extension); the remaining pressure distributions were obtained with mixing duct B. In all tests, the back pressure was much lower than the last static pressure measured in the duct, indicating that the flow was choked at the duct exit plane (independent of back pressure).

The values shown in Fig. 9 for the initial static pressure ratio ( $p_1/p_{Oa}$ ) are not measured points because no static pressure tap was located exactly at the rocket exit plane (Station 1). The initial static pressure was obtained by constructing a smooth curve through the static pressures measured along the mixing duct entrance (Fig. 3) and along the conical mixing duct. The value of this curve at  $x = 0$  was taken to be  $p_1$ .

The flow parameters ( $p_{Oa}/p_{Oj}$ ,  $w_a/w_j$ , and  $F_D/F_j$ ) are tabulated in Fig. 9 to facilitate comparisons. Individual firings on test conditions 2 and 3 are plotted in Figs. 9b and c to illustrate the small scatter of the data for the same nominal conditions and also to show the validity of obtaining exit plane profiles by means of composite plots of the various firings at the same nominal conditions.

The wall pressure distributions shown in Figs. 9b through f (for mixing duct B) all have similar shapes. The wall pressure initially decreased because of the pluming of the rocket stream, reaching a minimum at  $x/D_1 \approx 0.5$ . The wall pressure then increased to about  $p_1$  at  $x/D_1 \approx 1$  to 1.5. The pressure then remained approximately constant through the remainder of the conical portion of the duct. Downstream of the transition point between the conical and cylindrical sections ( $x/D_1 = 2.58$ ), the wall pressure dropped gradually to  $p_{Oa}/p_{Oj} \approx 0.55$  to 0.60 at the last measuring station in the duct.

#### 3.1.4 Pitot Pressure Profiles

The radial distributions of the pitot pressure at the duct exit are shown in Figs. 10a and b for test conditions 2 and 3. Significant scatter of the data is observed near the flow centerline where the flow is supersonic. Such scatter is inevitable because all of the experimental parameters could not be exactly duplicated from test to test. The flagged and unflagged symbols in Figs. 10a and b represent measurements taken on opposite sides of the flow centerline. The flow centerline was displaced approximately 0.1 in. from the duct centerline and was determined by making a best fit of the flagged and unflagged symbols.

Radial distributions of the pitot pressure at the duct exit are shown in Figs. 10c through e for test conditions 4 to 6, each of which consisted of a single rocket firing.

### 3.1.5 Gas Composition Profiles

Radial distributions of the gas composition at the duct exit are shown in Fig. 11 for test condition 2. Gas sample data were not obtained for the other points in the downstream choking mode. The solid lines shown in Fig. 11 were faired through the data to illustrate the trends. As was the case with the pitot-pressure profiles, the flagged and unflagged symbols represent data taken on opposite sides of the flow centerline.

## 3.2 BACK PRESSURE DEPENDENT EXPERIMENTS

Data from a series of experiments in the back pressure dependent mode of operation are presented in Table III and Figs. 12 through 14. All these experiments were made with mixing duct B (6-in. extension).

The parameters presented in Table III are identical with those presented in Table I, with the addition of the back pressure ratio and the diffuser (or spray section) pressure ratio. The back pressure was measured in the 12-in. -diam instrumentation section (Fig. 3), and the diffuser pressure was measured in the 24-in. -diam spray section.

### 3.2.1 Wall Pressure Distributions

Axial distributions of the duct wall static pressure are shown in Figs. 12a through g. Each figure presents data for a single rocket firing. The lower limit of  $p_b/p_{0a}$  corresponds to the pressure measured in the 12-in. -diam instrumentation section, and the upper limit corresponds to the pressure measured in the spray section. The range of the two measurements is presented because there seems to be some consistent, but unexplainable, error in the measurement in the instrumentation section (that pressure being 0.2 to 0.6 psi lower than the spray section pressure). If the pressure measured in the instrumentation section were correct, then a very large favorable pressure gradient would occur just upstream of the mixing duct exit (Fig. 12f, for example). It is not conceivable how such large axial pressure gradients could occur in an unchoked flow. The pressure measured in the spray section, on the other hand, agrees well in all cases with the pressure obtained by extrapolating the mixing duct wall pressure distribution to the duct exit.

The results shown in Figs. 12a and e represent experiments which were only slightly influenced by back pressure, compared with the experiments in the downstream choking mode. This small influence of  $p_b$  can be illustrated by comparing Figs. 12a and 9b and comparing Figs. 12e and 9c. For the other test conditions presented in Fig. 12, the duct flow was strongly dependent on the back pressure.

### 3.2.2 Pitot Pressure Profiles

Radial distributions of pitot pressure at the duct exit are shown in Fig. 13 for test conditions 8, 9, 10, 12, and 13. The pitot pressures near the duct centerline were not recorded for test condition 10 (Fig. 13c).

### 3.2.3 Gas Composition Profiles

Radial distributions of gas composition at the duct exit are shown in Fig. 14 for test conditions 8, 9, and 10. The solid lines again are merely faired curves and should be considered only as an approximate guide to the trends.

## 3.3 COMPARISON OF UPSTREAM CHOKING AND DOWNSTREAM CHOKING MODES

It was pointed out in Section I that the downstream choking mode would appear to be the most attractive operational mode for the mixing duct of an air-augmented rocket. The desirability of the downstream choking mode can be illustrated by comparing the performance of the basic conical mixing duct (Ref. 3) with the performance of the same conical duct with a 6-in. -long cylindrical extension (duct configuration B of this investigation). The rocket engine used in the experiments reported in Ref. 3 was slightly different from the engine used in the experiments on duct configuration B. The differences, however, were small and do not invalidate a direct comparison of the experimental results for mass flow ratio and duct thrust.

The mass flow ratio ( $w_a/w_j$ ) is shown in Fig. 15a for the two duct configurations. For a given value of the stagnation pressure ratio ( $p_{Oa}/p_{Oj}$ ), the mass flow ratio is typically 10 percent less for duct configuration B (downstream choking mode) than for the basic conical mixing duct of Ref. 3 (upstream choking mode).

The mixing duct thrust ratio ( $F_D/F_j$ ) is shown in Fig. 15b for the two duct configurations. The duct thrust ratio is typically 50 to 60 percent higher for duct configuration B than for the basic conical duct.

The mixing duct thrust ( $F_D$ ) is indicative of the gross thrust of the mixing duct of an air-augmented rocket. The net thrust of the duct is  $F_D$  minus the inlet and external drag. One would expect the inlet and external drag to be approximately the same for the two configurations,

and the net thrust comparison would be even more favorable to operation in the downstream choking mode. It should be noted that the very important aspect of mixing duct weight is not considered in this comparison.

#### SECTION IV CONCLUDING REMARKS

Results from a series of ducted mixing and burning experiments have been presented. Twenty-six rocket firings were made in this test series. The ducted mixing system was operated in the downstream choking mode (independent of back pressure) for 19 of these firings; the mixing system was back pressure dependent for the remaining rocket firings. Data presented include axial distributions of the wall static pressure and radial distributions of gas composition and pitot pressure at the mixing duct exit.

The experimental results for the mixing duct used in this investigation (operated in the downstream choking mode) have been compared to the results reported in Ref. 3 for a shorter mixing duct which operated in the upstream choking mode. This comparison clearly indicates that, for certain propulsion applications, it is desirable to make the mixing duct long enough to operate in the downstream choking mode.

The experiments presented in this report are part of an extensive theoretical and experimental investigation of the ducted turbulent mixing of coaxial streams. These and other experiments will be correlated with theory in a forthcoming AEDC report.

## REFERENCES

1. Perini, L. L., Wilson, W. E., Walker, R. E., and Dugger, G. L. "Preliminary Study of Air Augmentation of Rocket Thrust." Journal of Spacecraft and Rockets, Vol. 1, No. 6, November/December 1964, pp. 626-634.
2. Staff Report. "Composite Engines." Space/Aeronautics, Vol. 48, No. 3, August 1967, pp. 83-90.
3. Peters, C. E., Peters, T., and Billings, R. B. "Mixing and Burning of Bounded Coaxial Streams." AEDC-TR-65-4, March 1965 (Available from DDC as AD458348).
4. Fabri, J. and Paulon, J. "Theory and Experiments on Supersonic Air-Air Ejectors." NACA-TM-1410, 1958.
5. Chow, W. L. and Addy, A. L. "Interaction between Primary and Secondary Streams of Supersonic Ejector Systems and Their Performance Characteristics." AIAA Journal, Vol. 2, No. 4, April 1964, pp. 686-695.
6. Smith, R. E., Jr. and Matz, R. J. "Verification of a Theoretical Method of Determining Discharge Coefficients for Venturis Operating at Critical Flow Conditions." AEDC-TR-61-8 (AD263714), September 1961.
7. Rhodes, R. P., Rubins, P. M., and Chriss, D. E. "The Effect of Heat Release on the Flow Parameters in Shock-Induced Combustion." AEDC-TR-62-78 (AD275366), May 1962.

**APPENDIXES**  
**I. ILLUSTRATIONS**  
**II. TABLES**

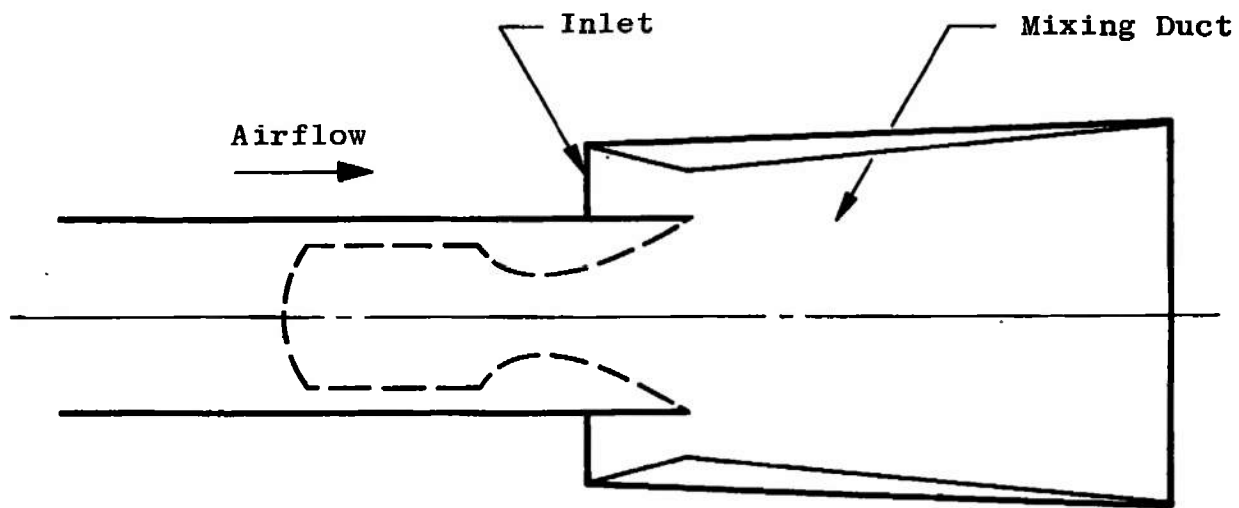
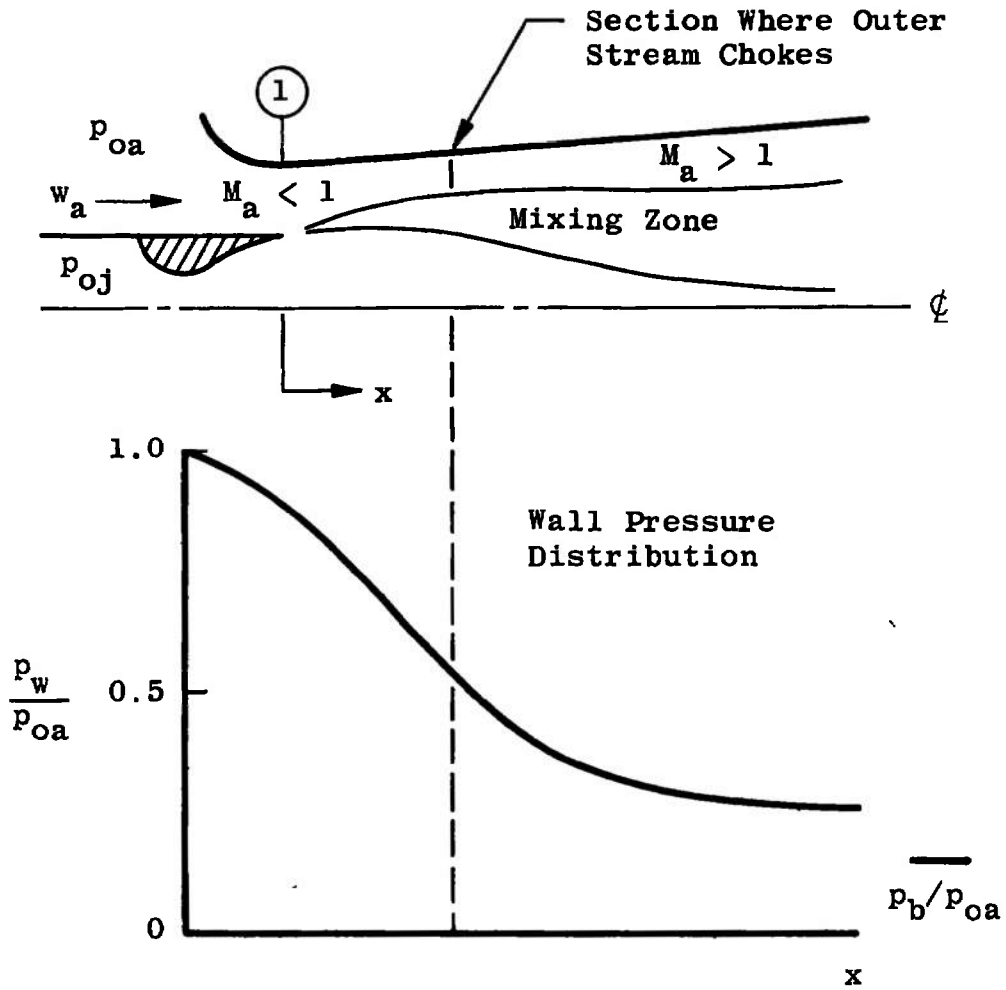
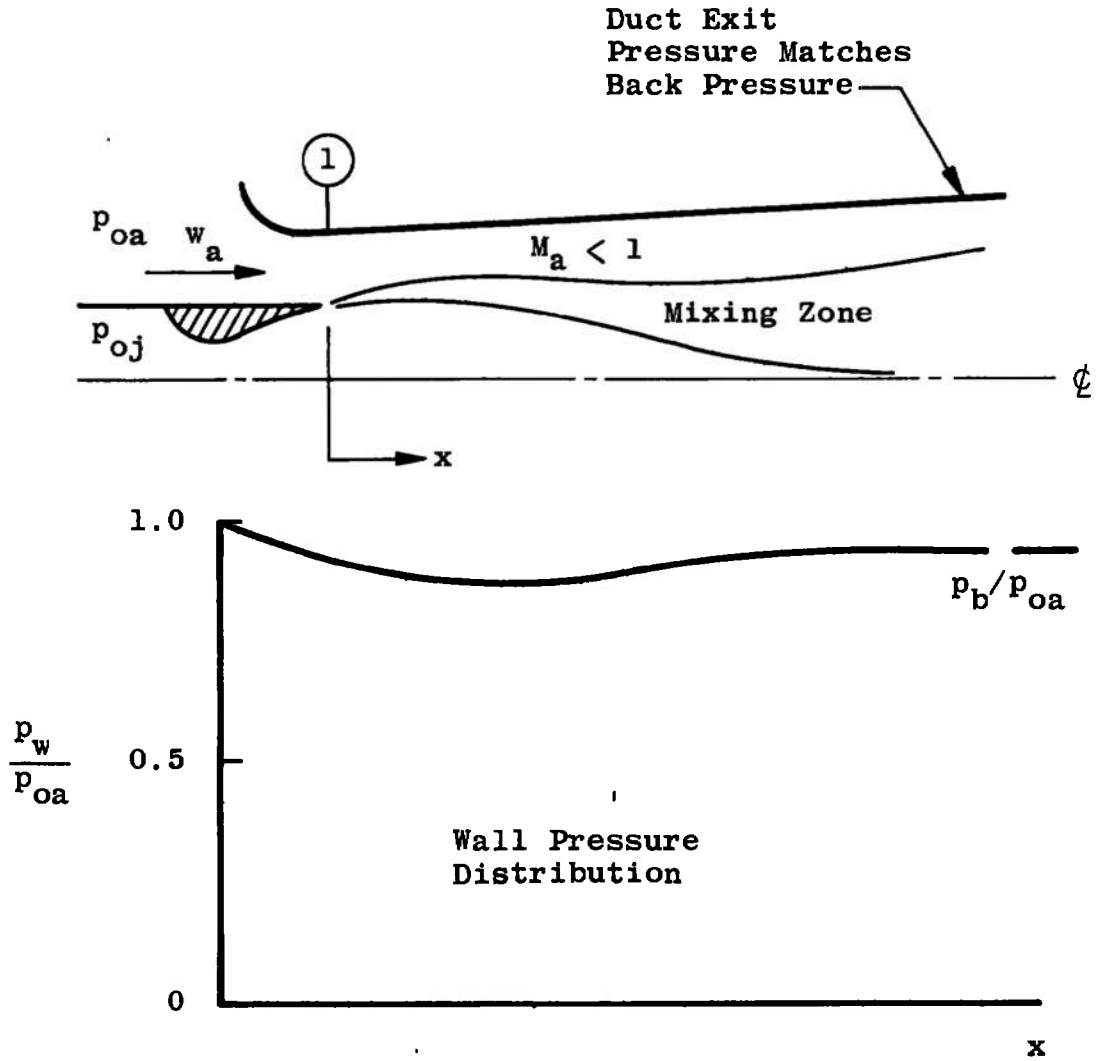


Fig. 1 Schematic of Air-Augmented Rocket

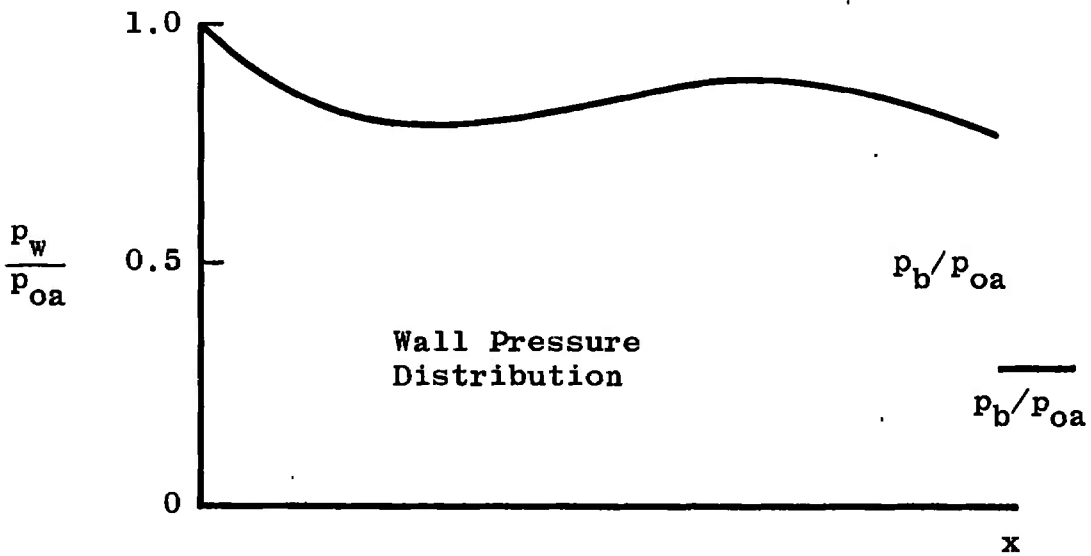
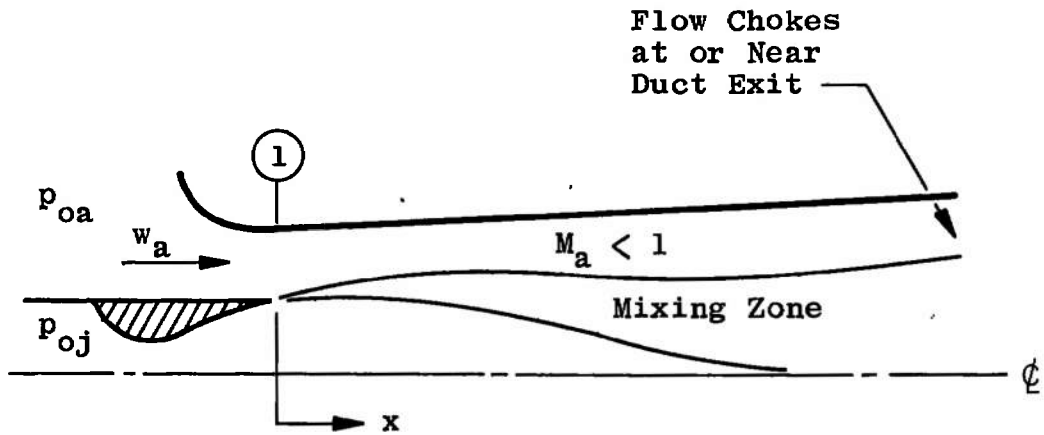


a. Upstream Choking Mode

Fig. 2 Operational Modes of a Ducted Mixing System



b. Back Pressure Dependent Mode  
 Fig. 2 Continued



c. Downstream Choking Mode  
Fig. 2 Concluded

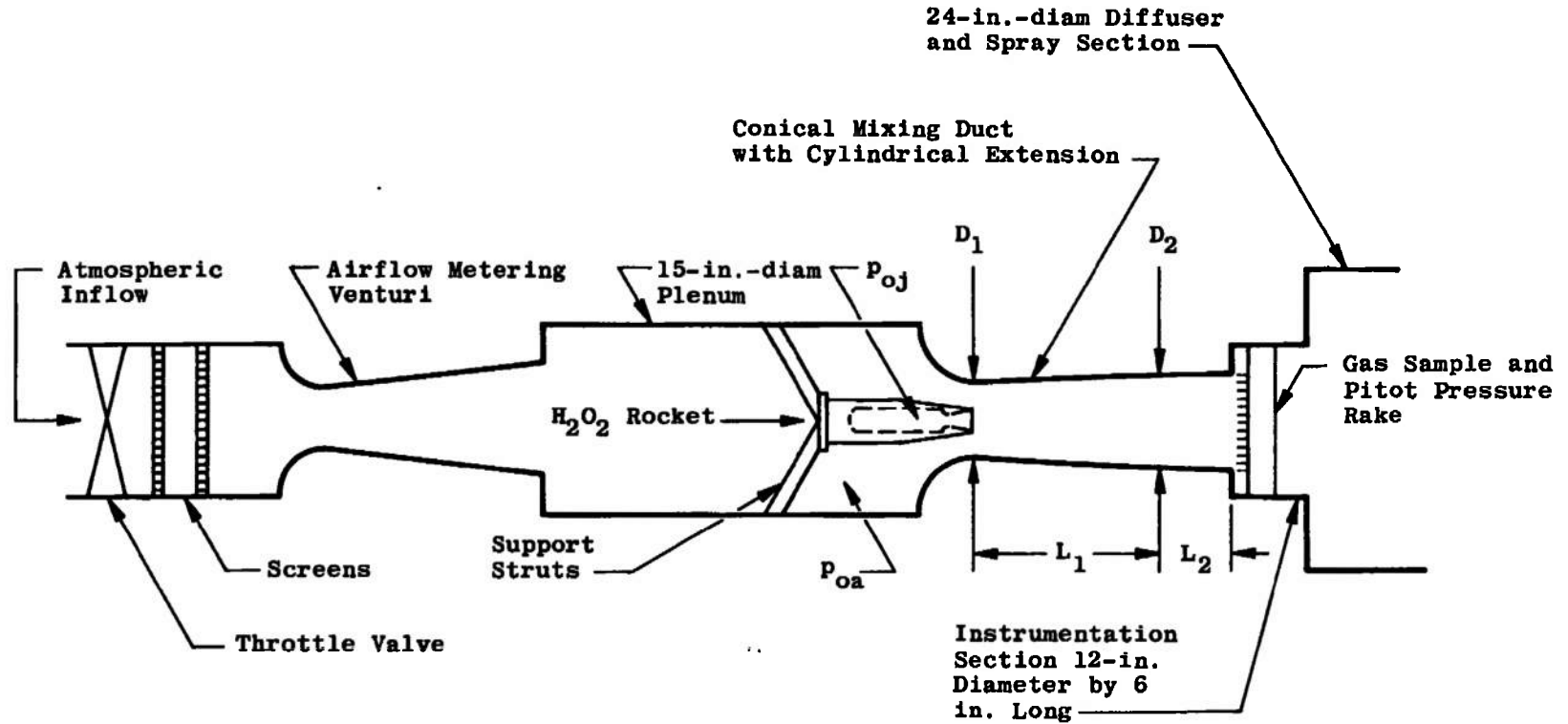


Fig. 3 Schematic of Propulsion Research Cell (R-1B)

20

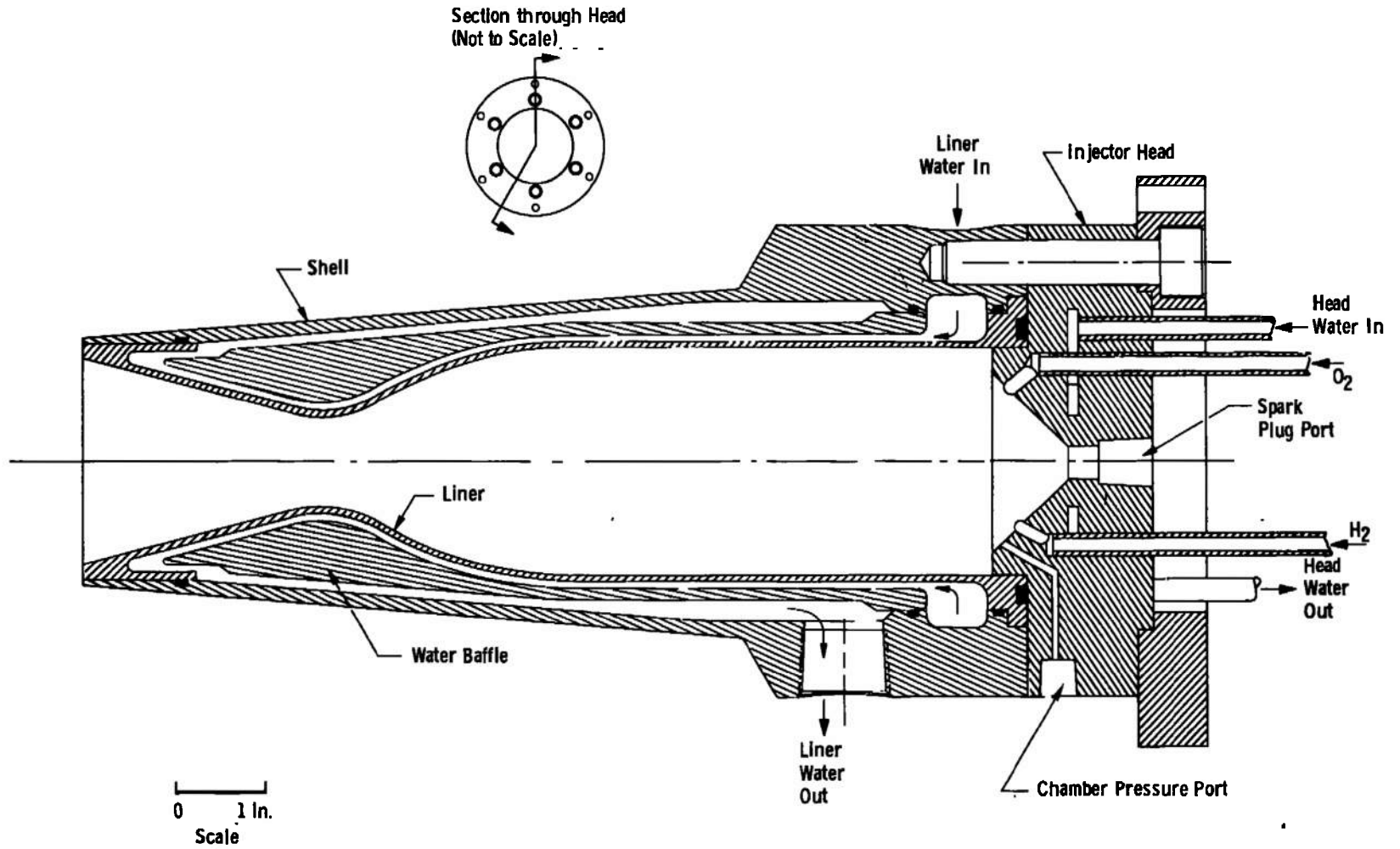


Fig. 4 Rocket Engine

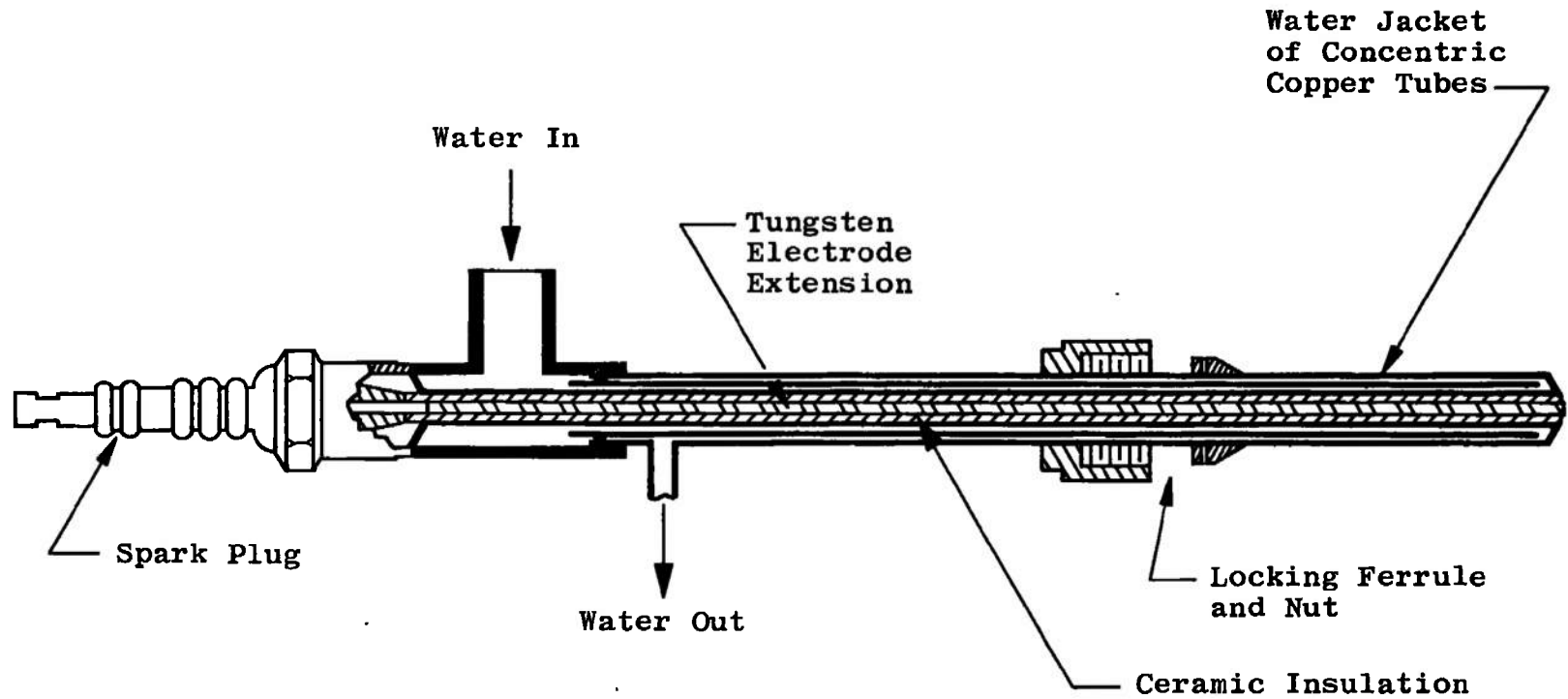
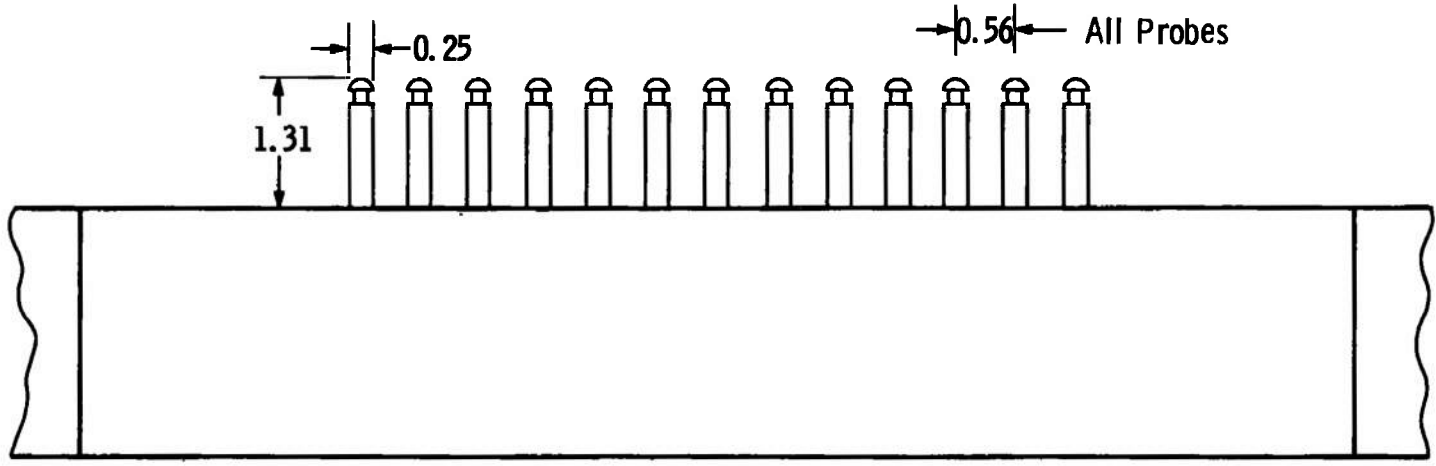
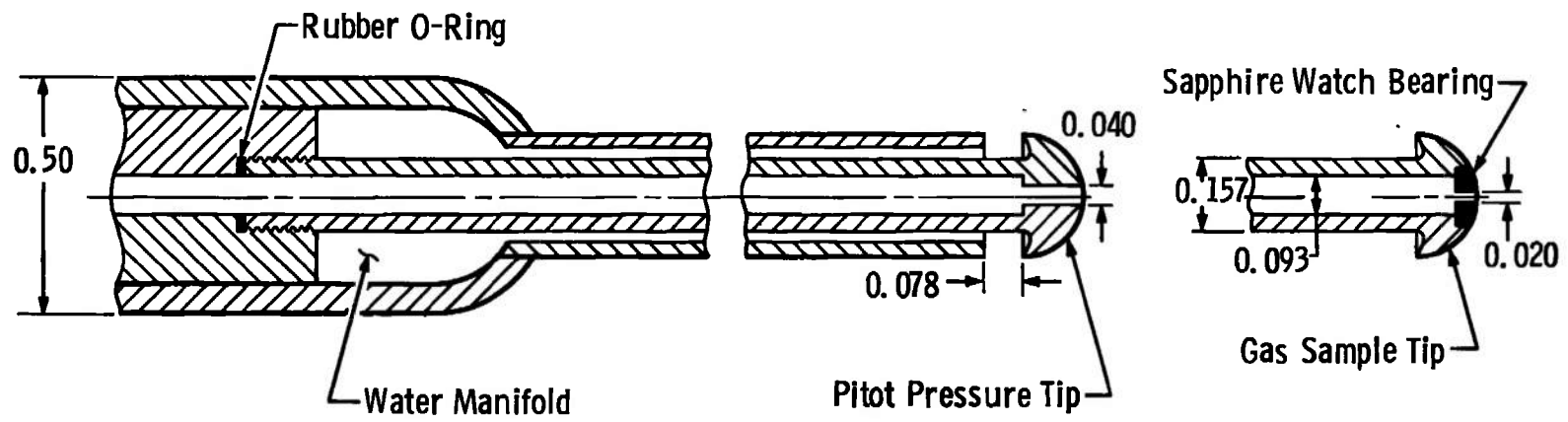


Fig. 5 Details of Water-Cooled Spark Plug



All Dimensions in Inches

a. Rake Geometry



b. Probe Tip Details  
Fig. 6 Concluded

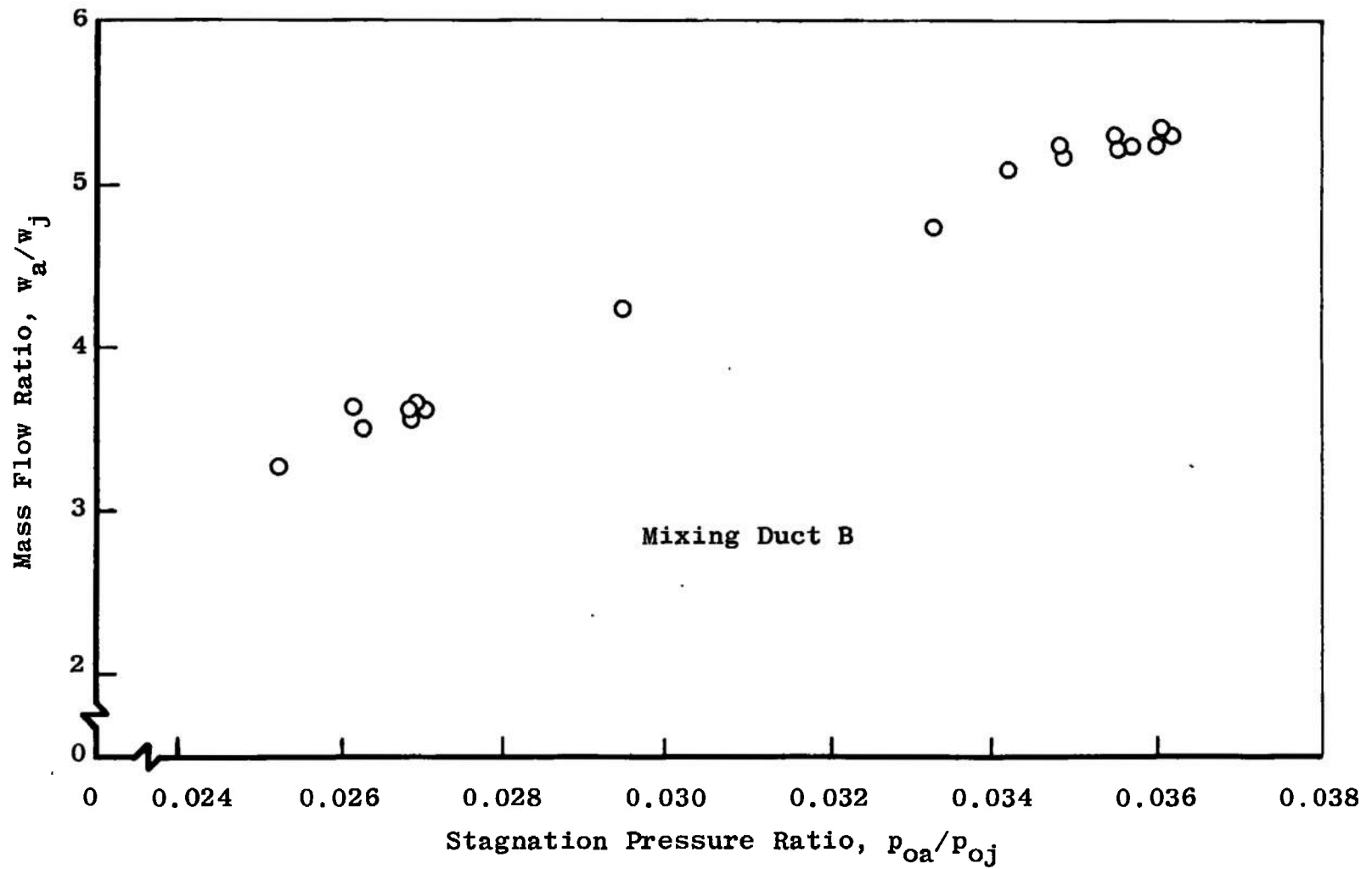


Fig. 7 Mass Flow Ratio, Downstream Choking Mode

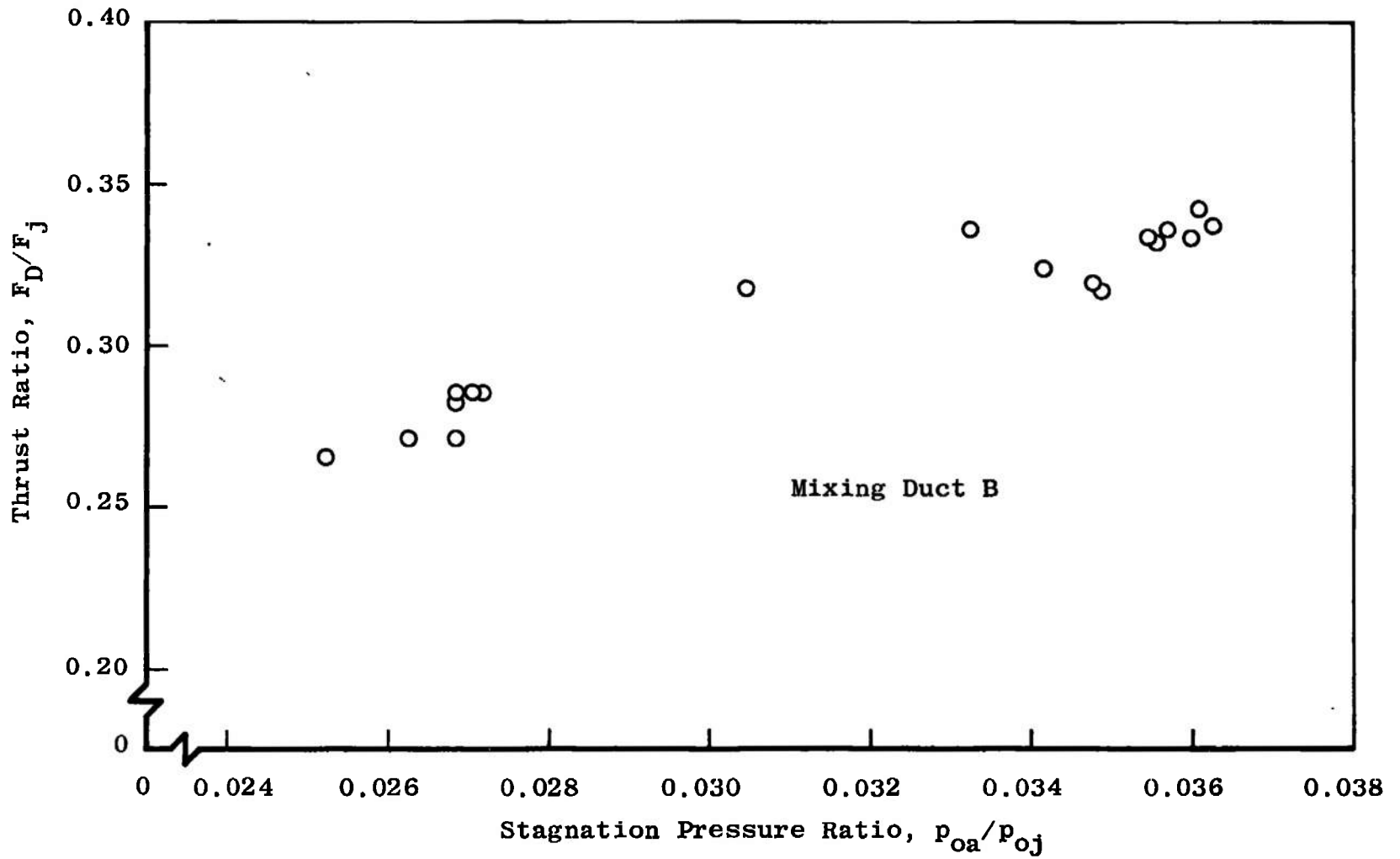
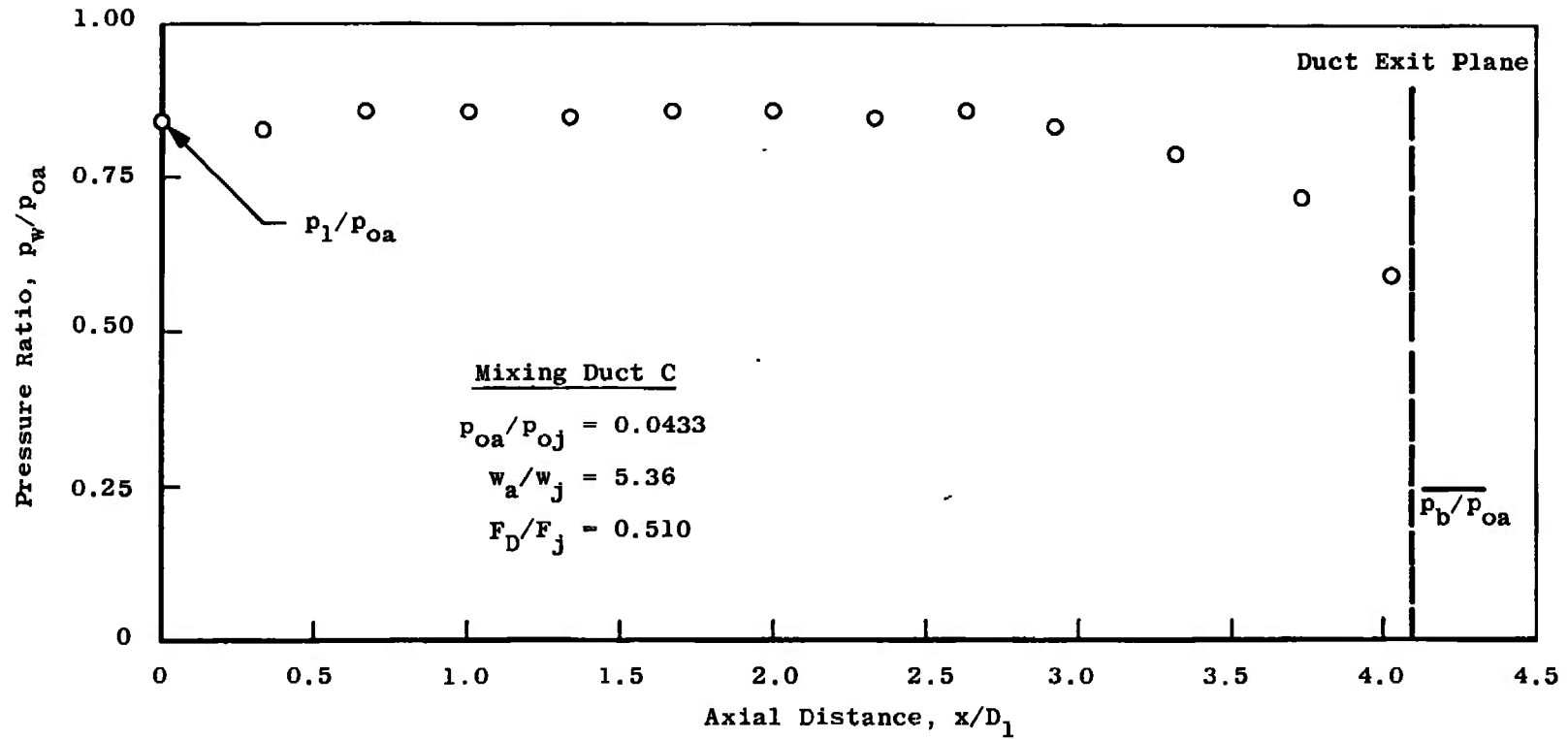
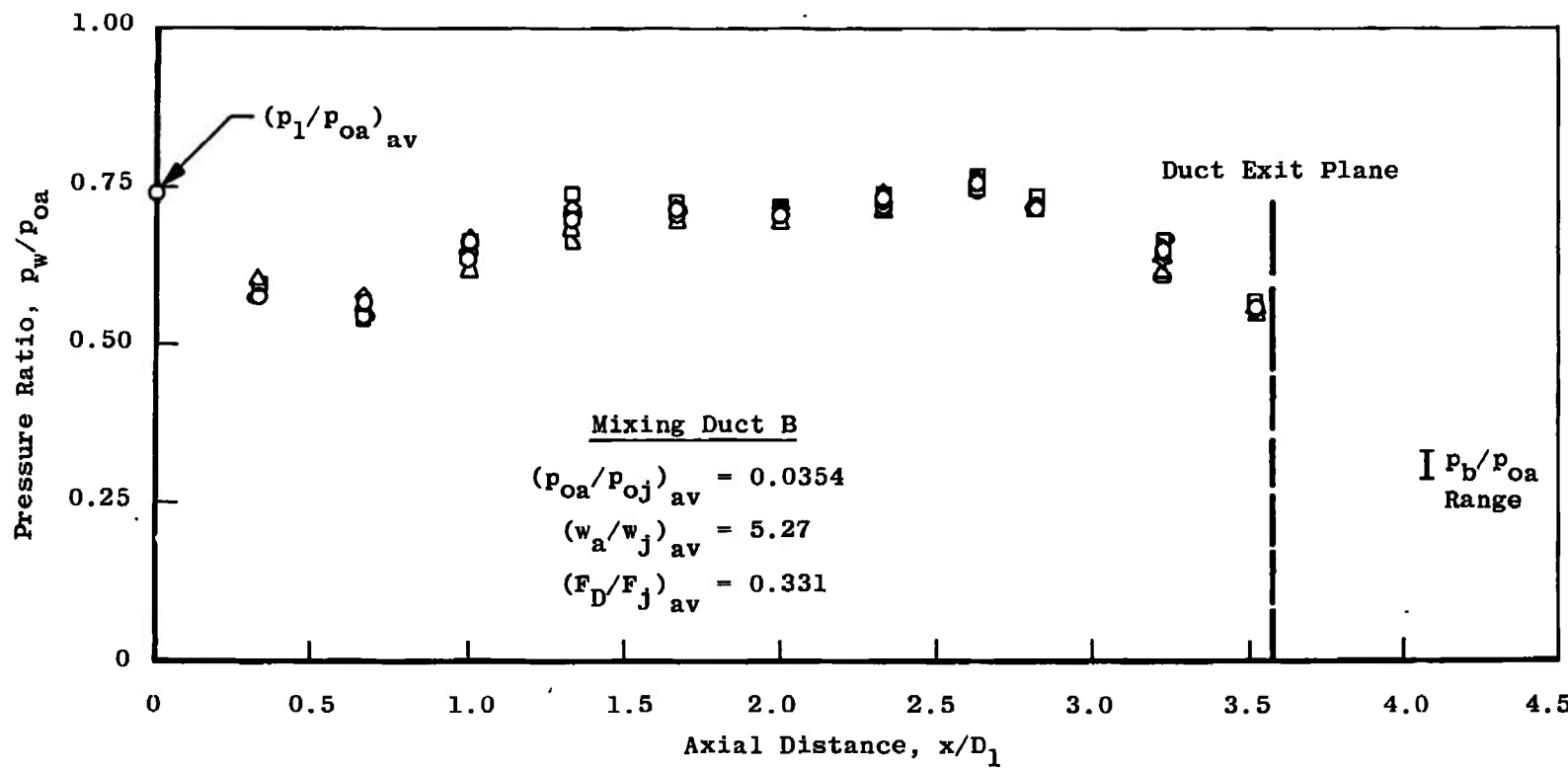


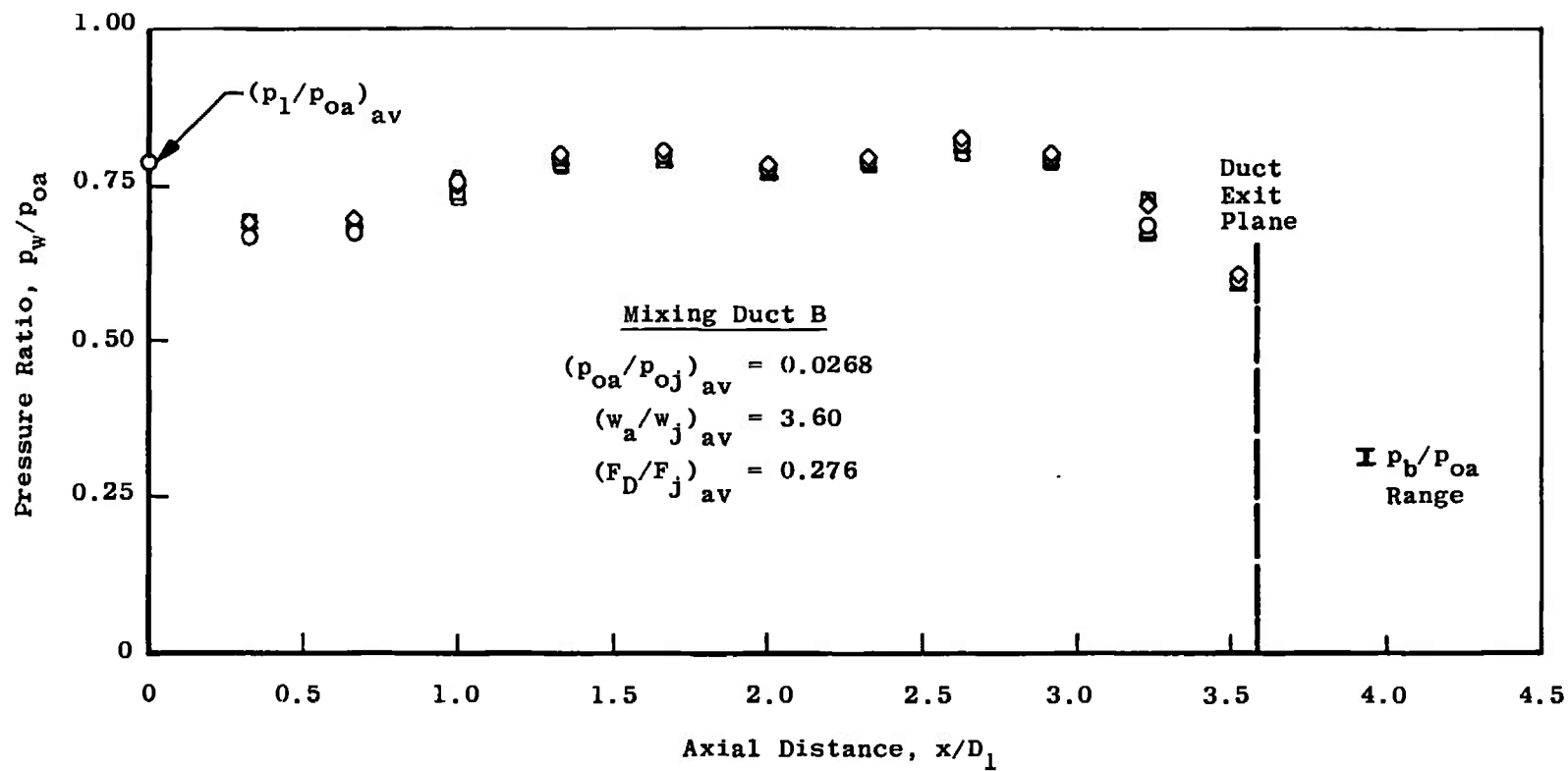
Fig. 8 Mixing Duct Thrust, Downstream Choking Mode



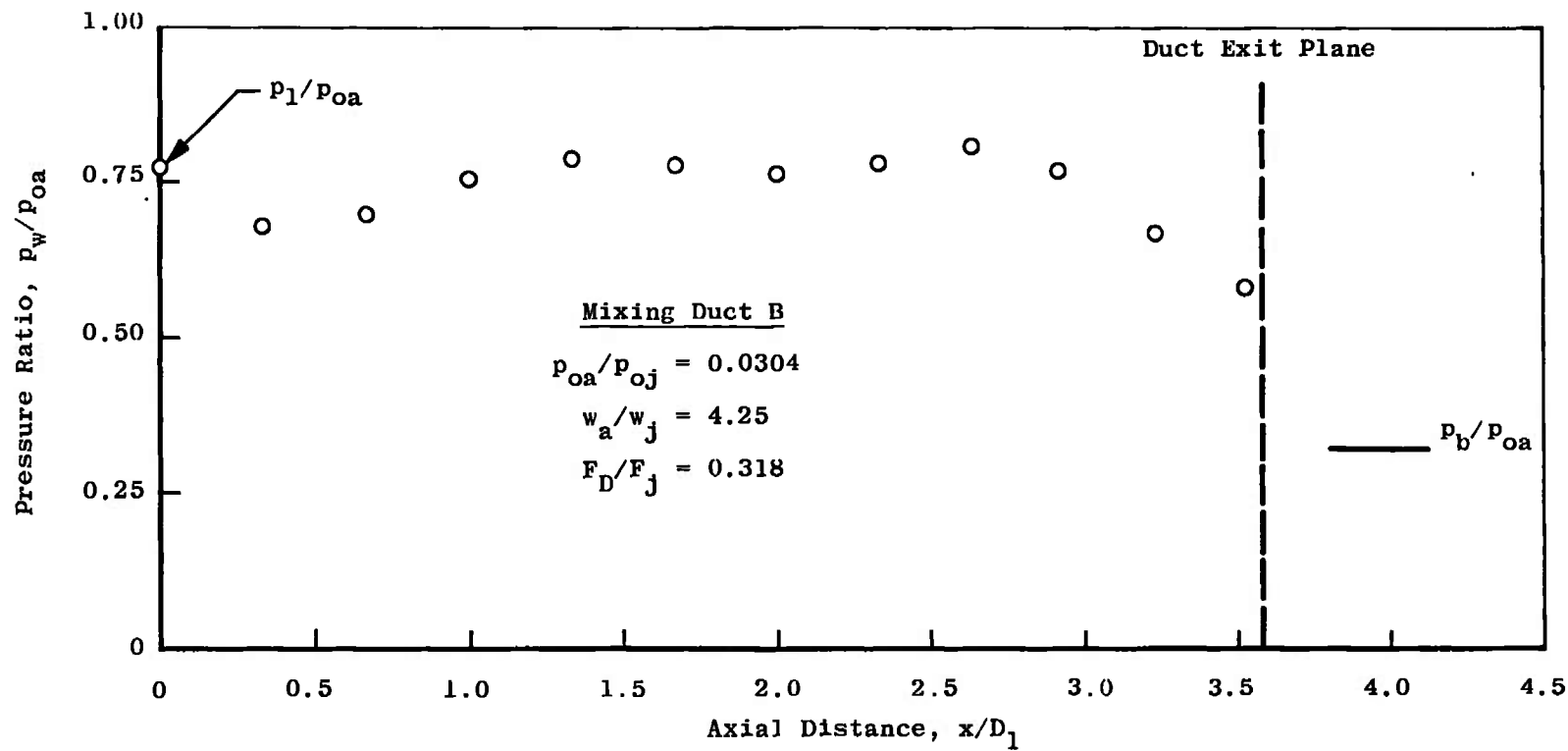
a. Test Condition 1  
**Fig. 9 Duct-Wall Pressure, Downstream Choking Mode**



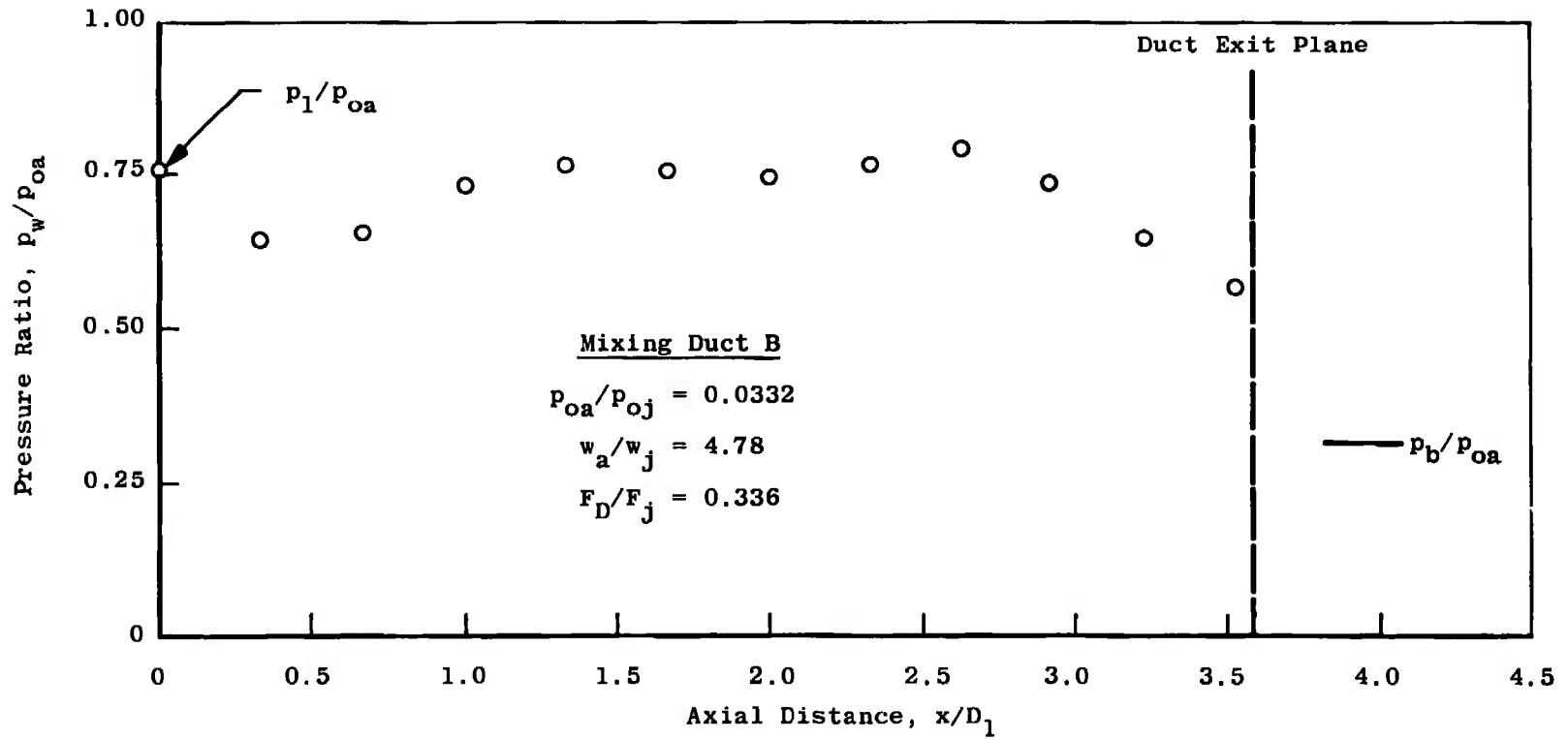
b. Test Condition 2  
 Fig. 9 Continued



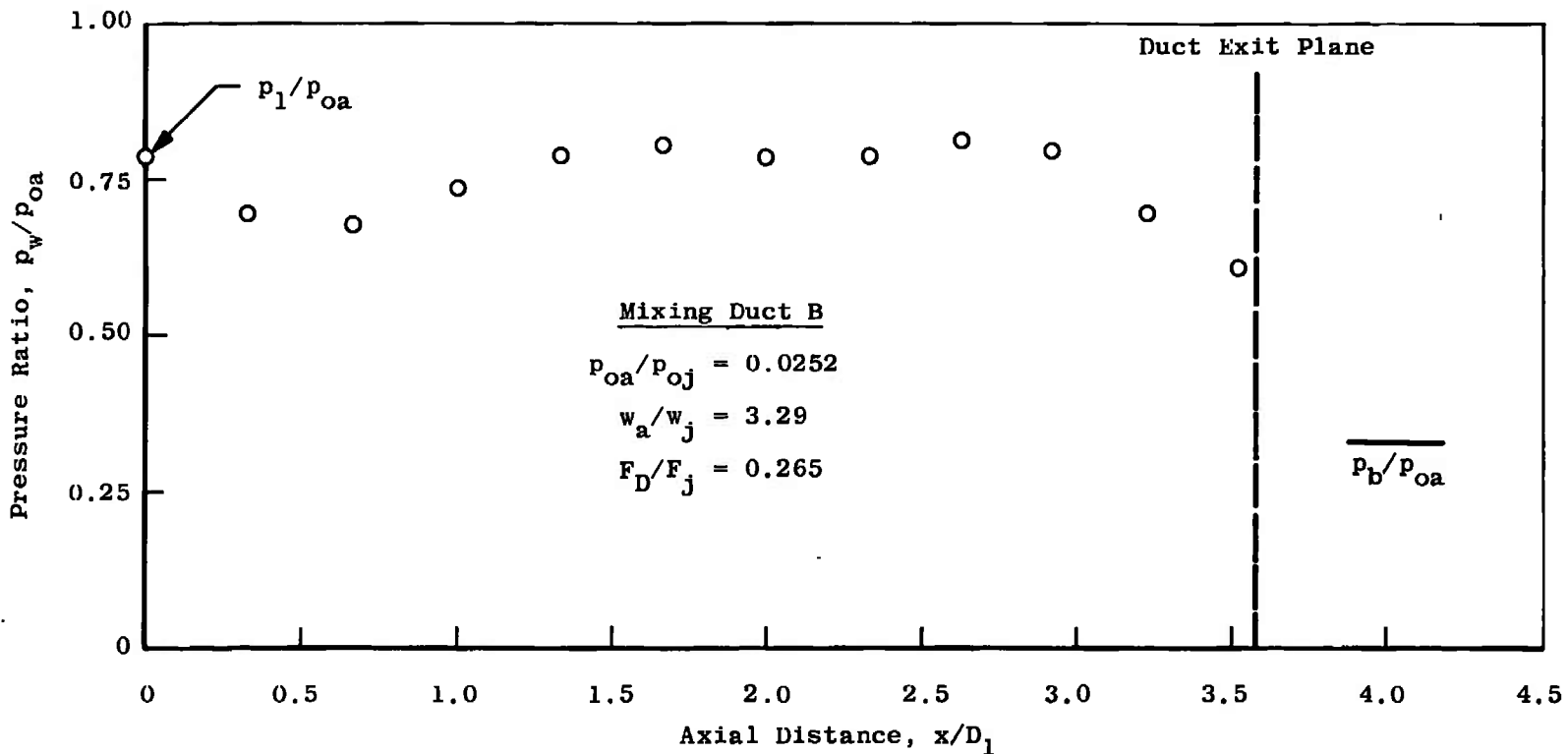
c. Test Condition 3  
Fig. 9 Continued



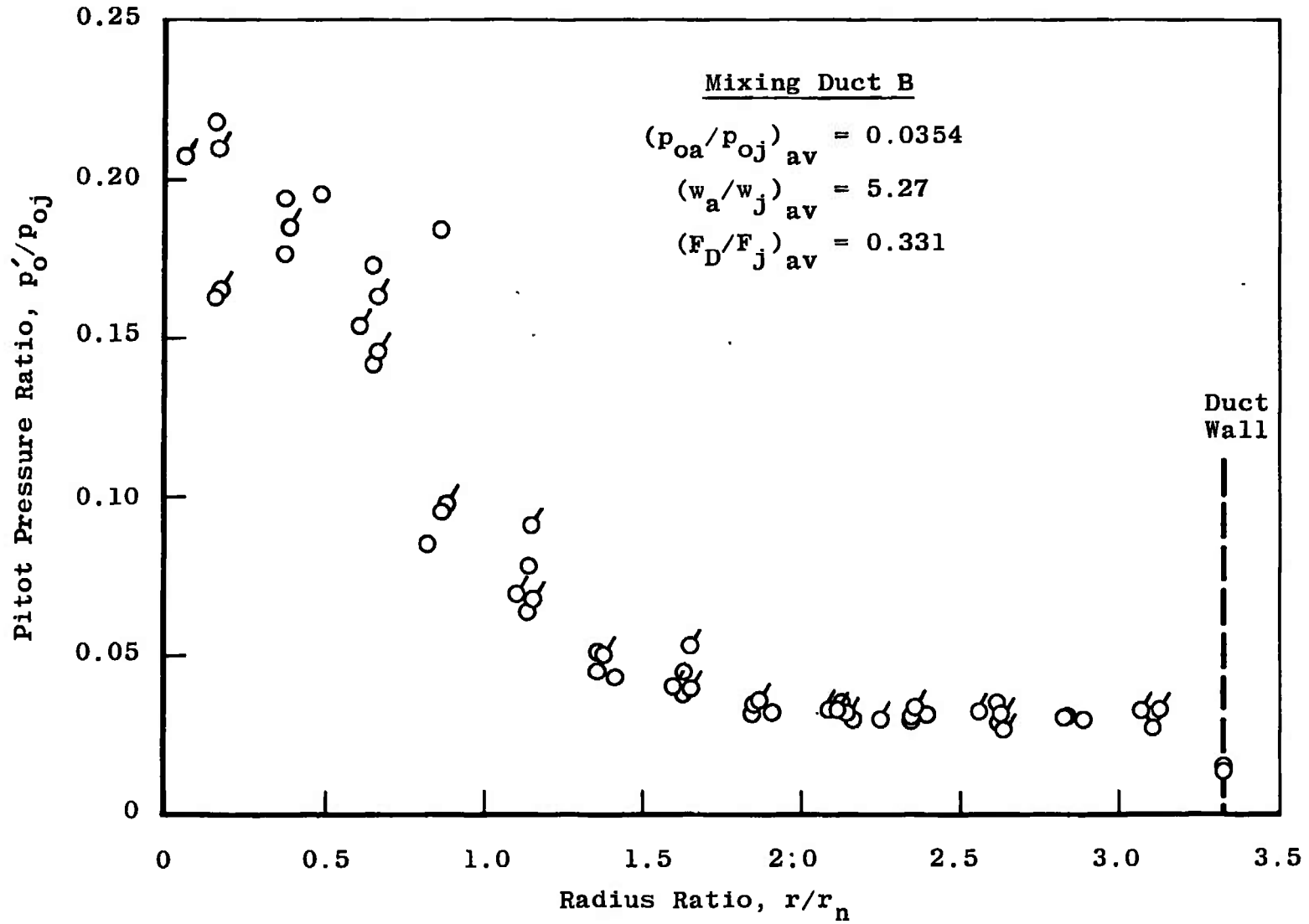
d. Test Condition 4  
 Fig. 9 Continued



e. Test Condition 5  
Fig. 9 Continued

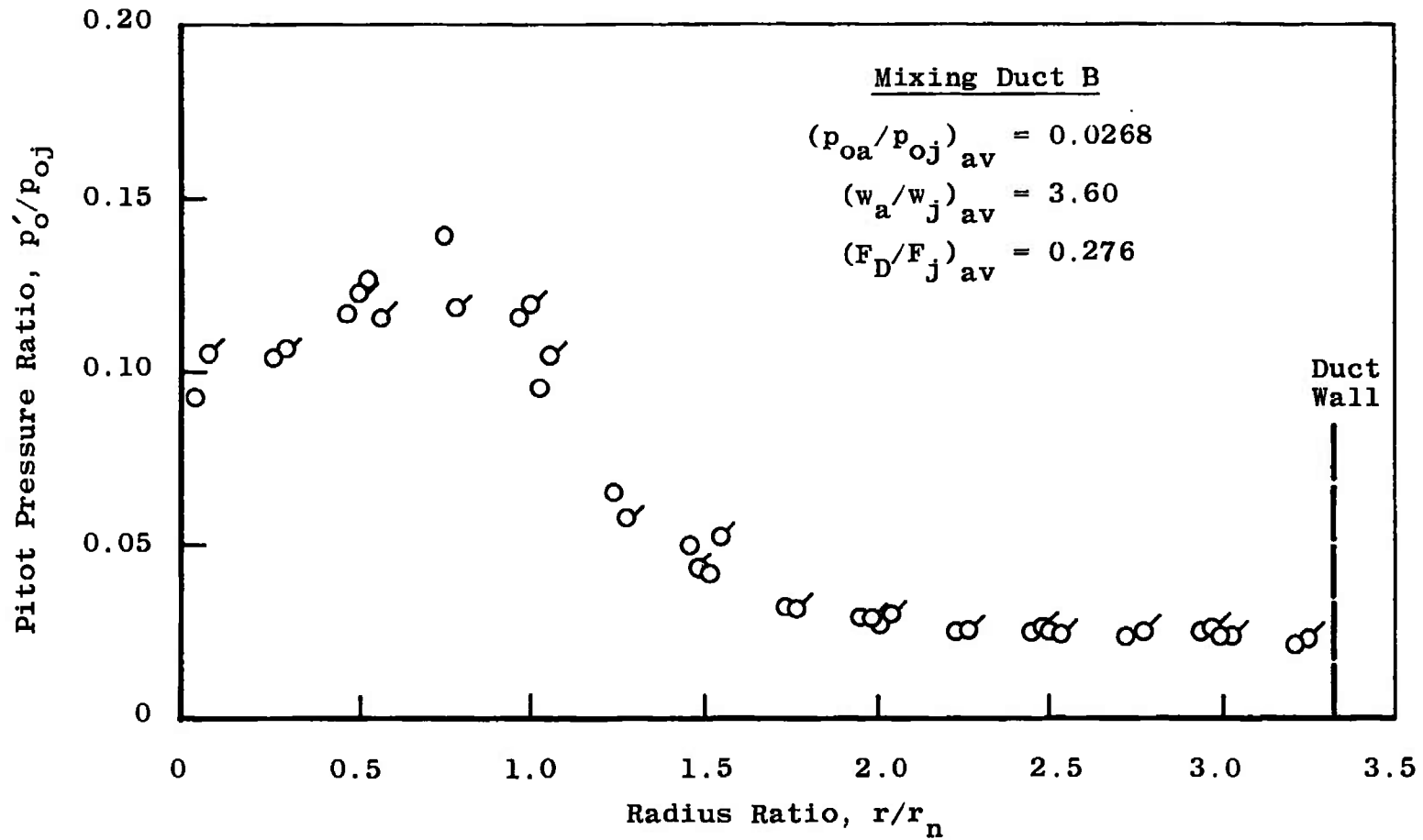


f. Test Condition 6  
 Fig. 9 Concluded

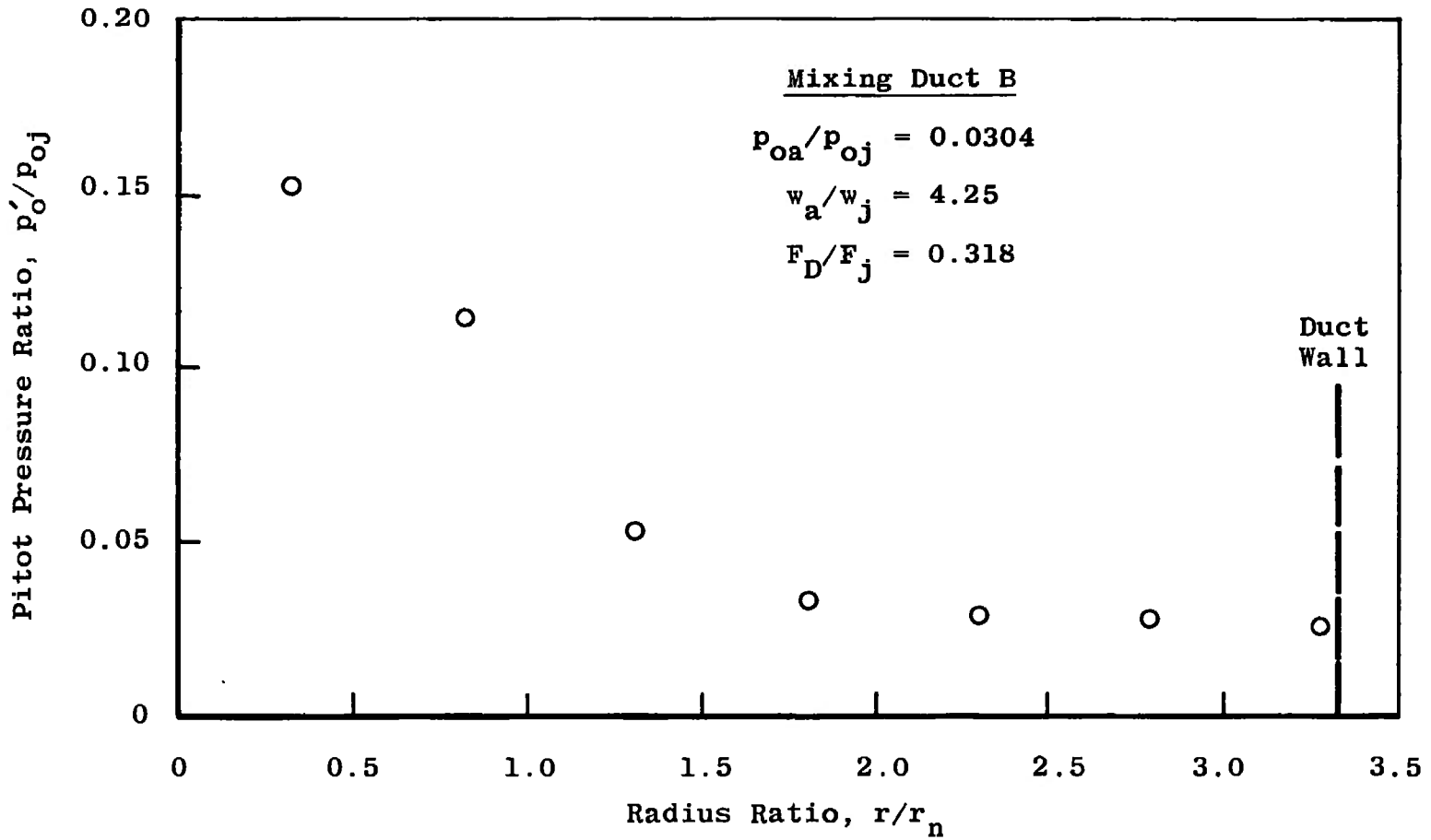


a. Test Condition 2

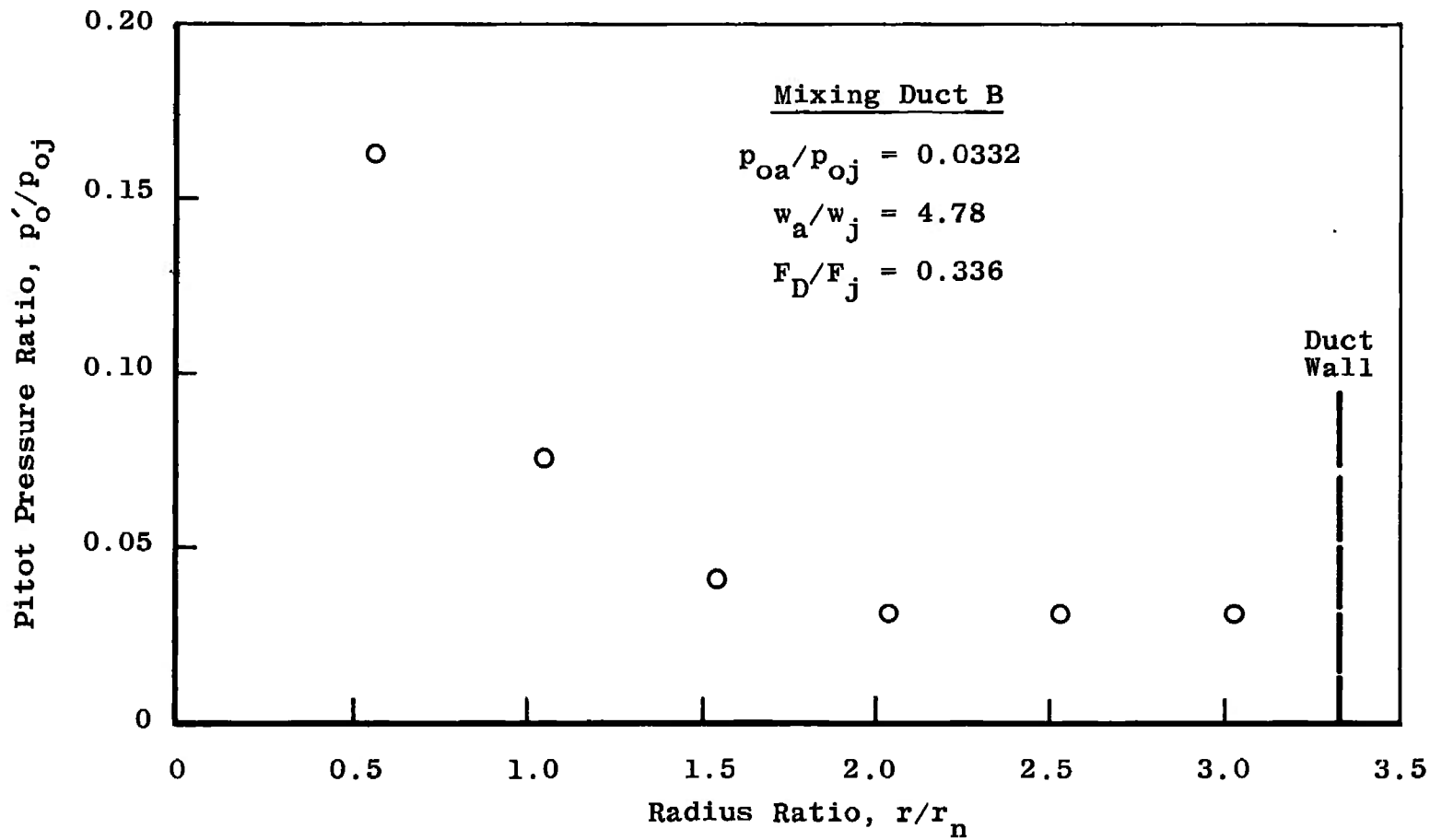
Fig. 10 Pitot Pressure at Duct Exit, Downstream Choking Mode



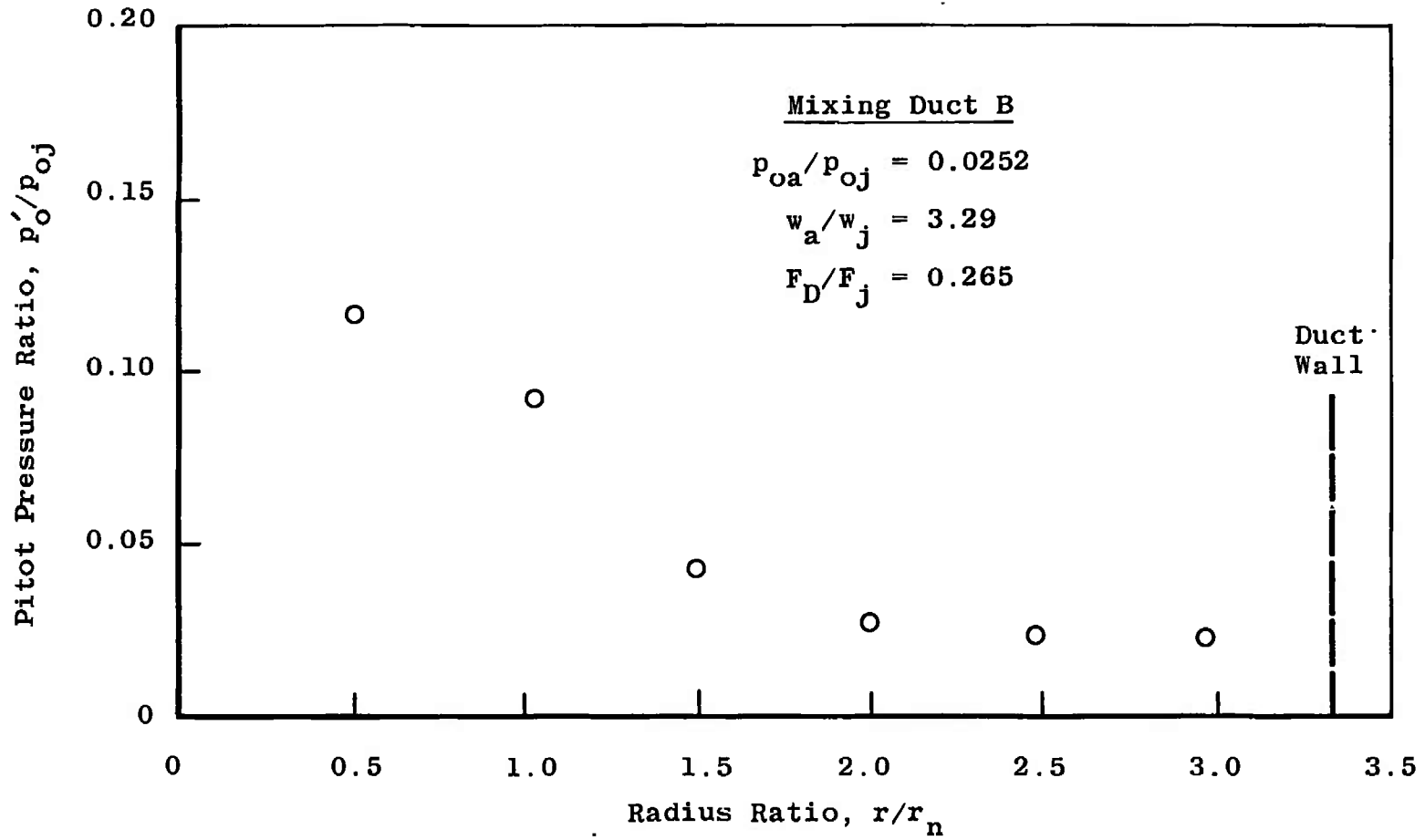
b. Test Condition 3  
 Fig. 10 Continued



c. Test Condition 4  
Fig. 10 Continued



d. Test Condition 5  
 Fig. 10 Continued



e. Test Condition 6  
Fig. 10 Concluded

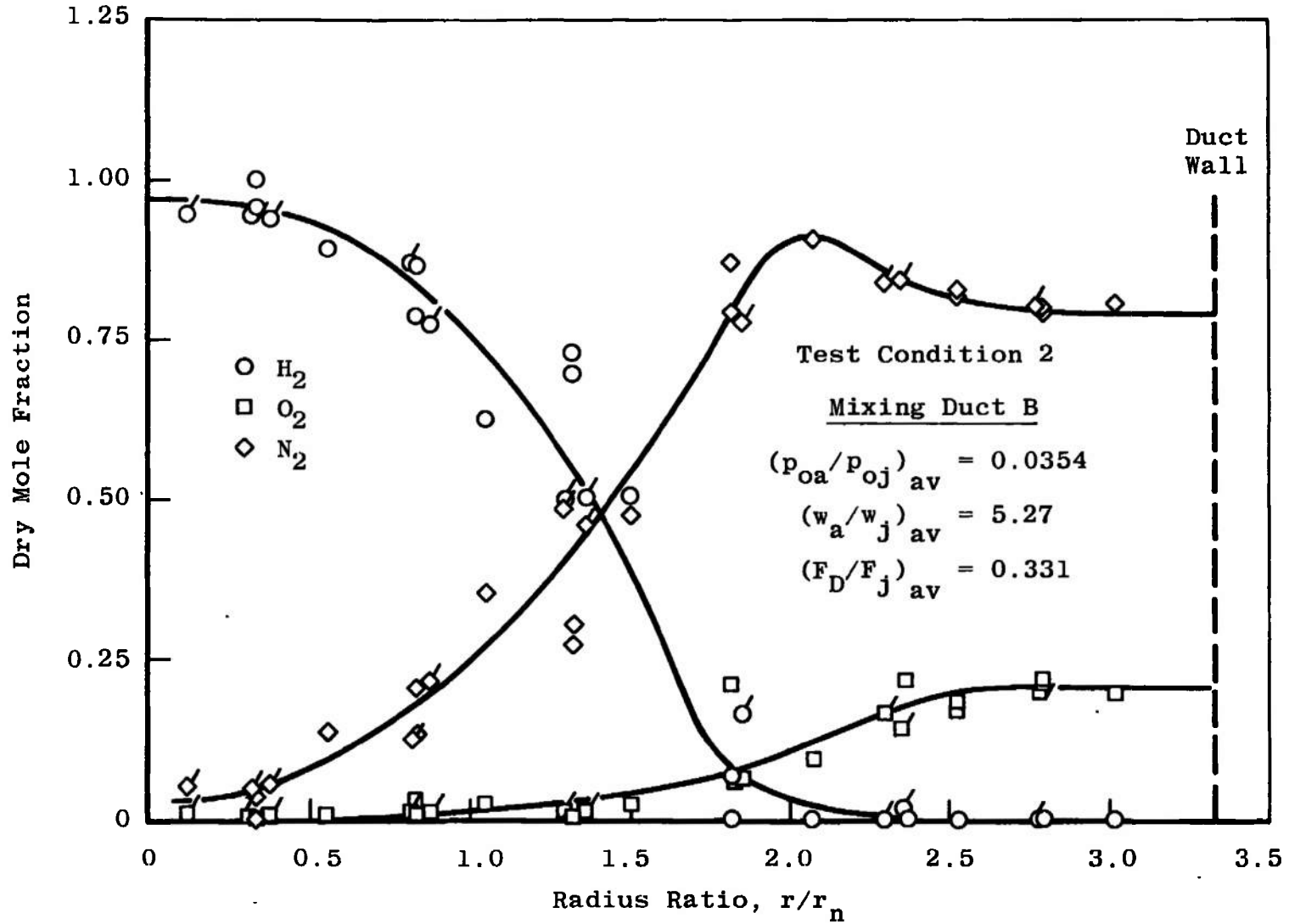
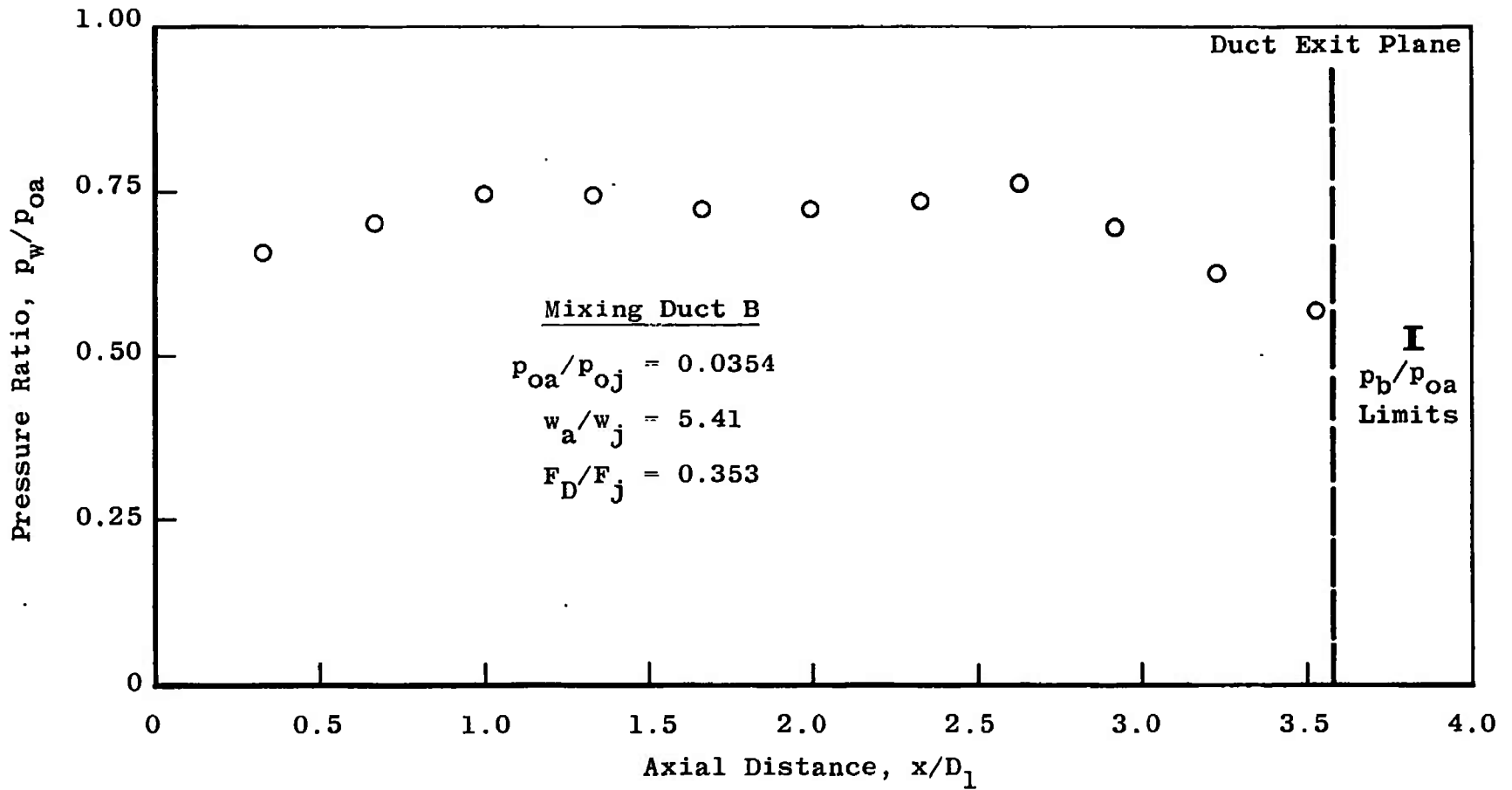


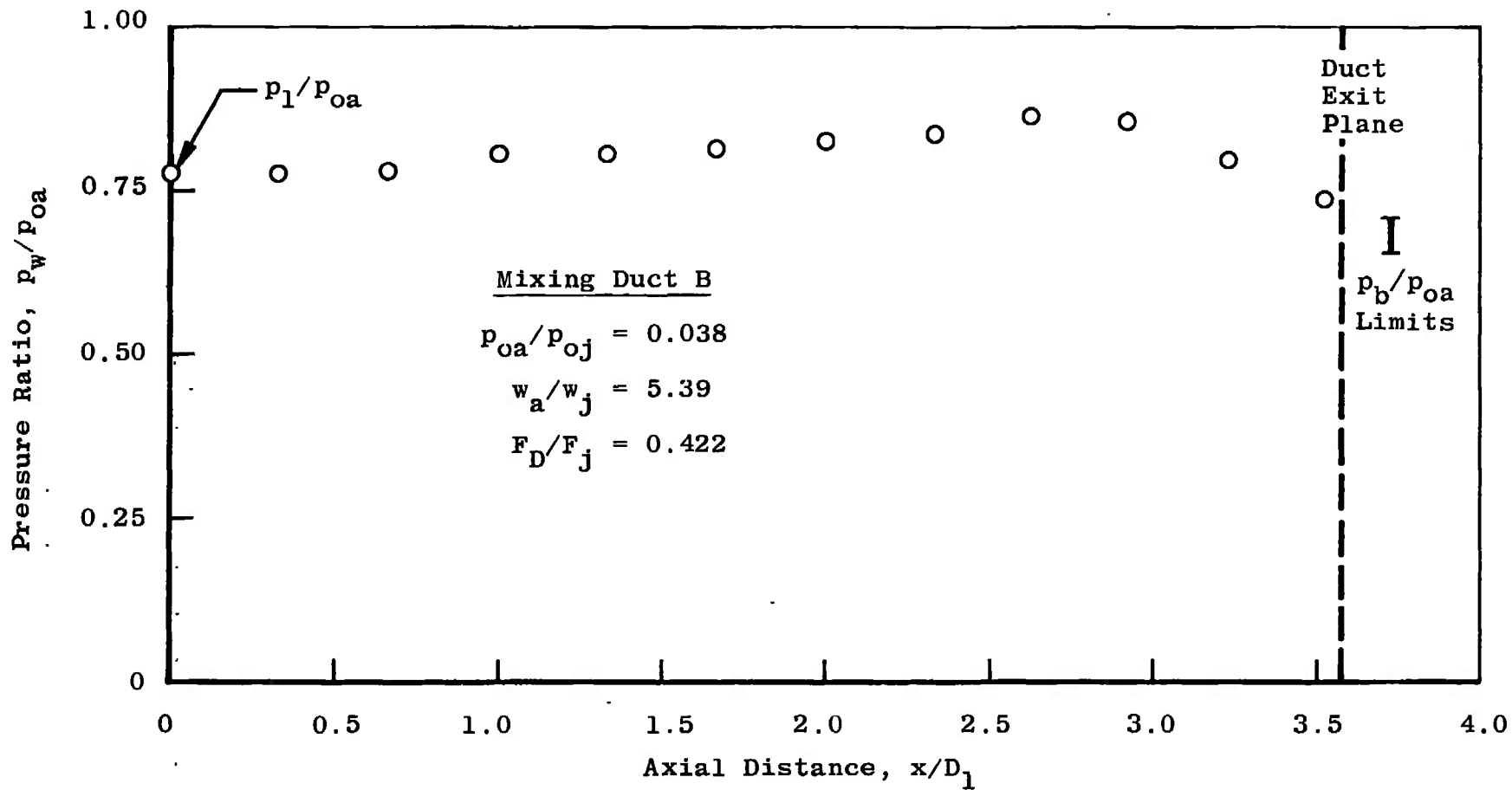
Fig. 11 Composition at Duct Exit, Downstream Choking Mode



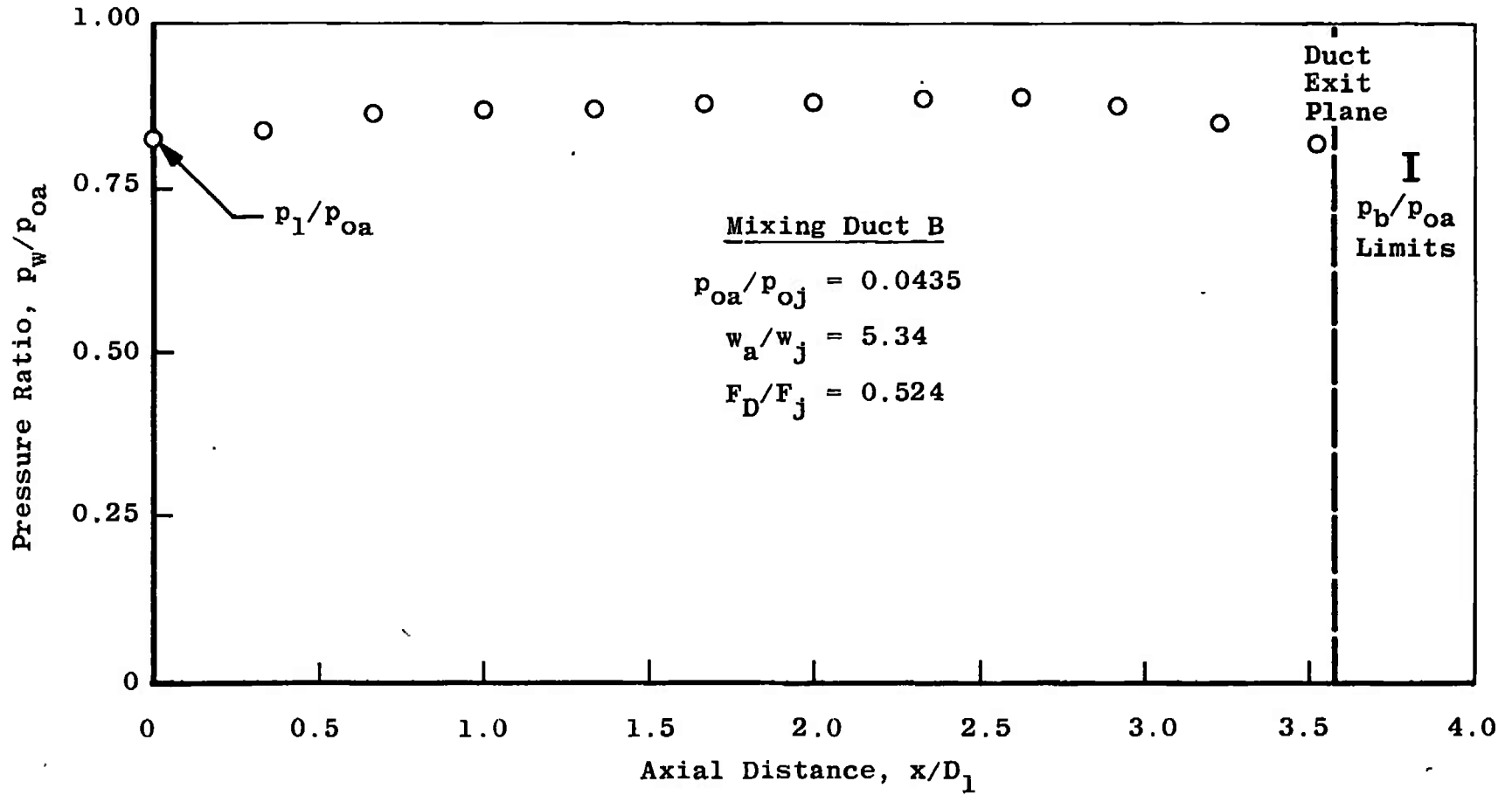
a. Test Condition 7

Fig. 12 Duct Wall Pressure, Back Pressure Dependent Mode

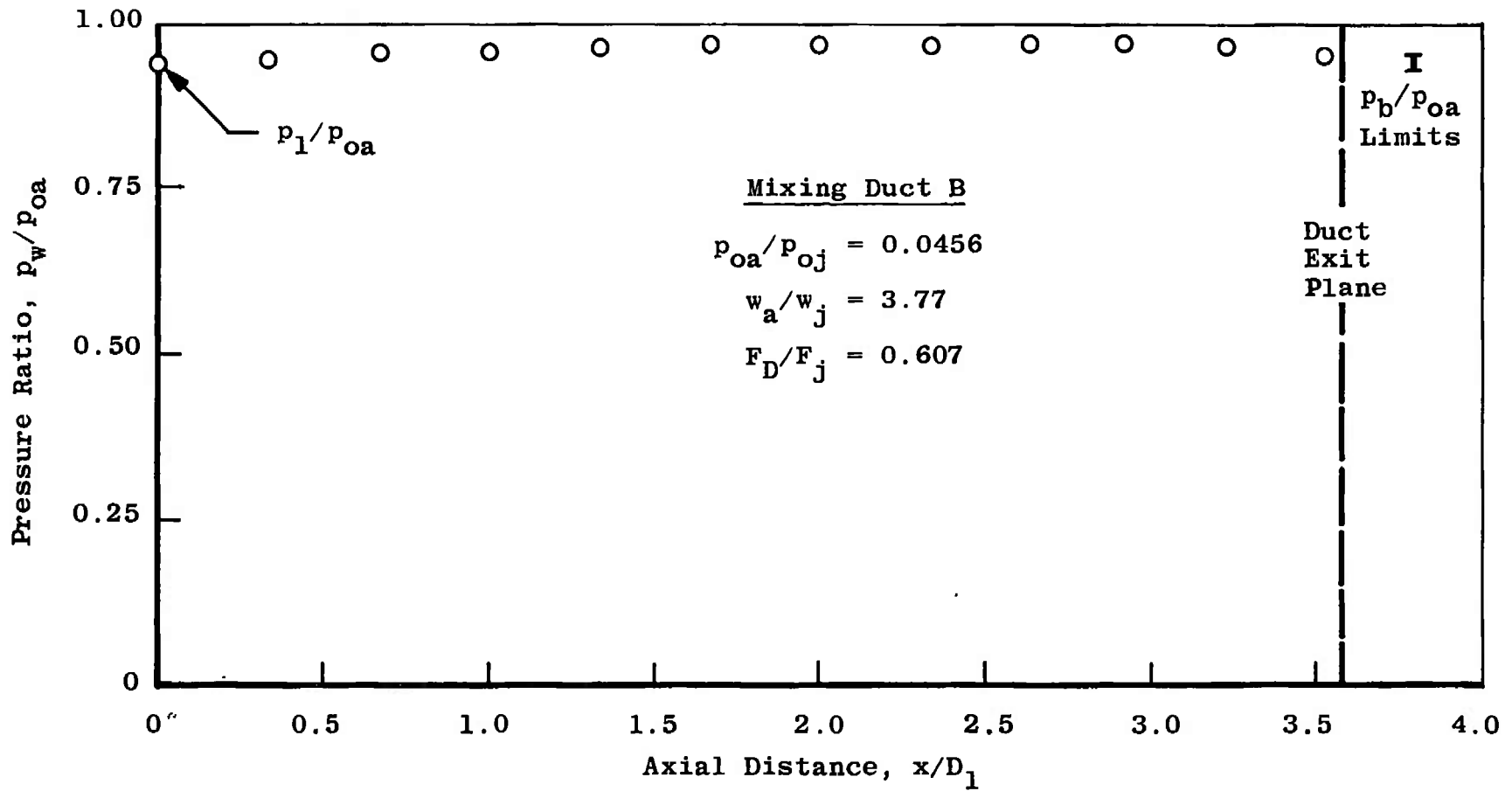
88



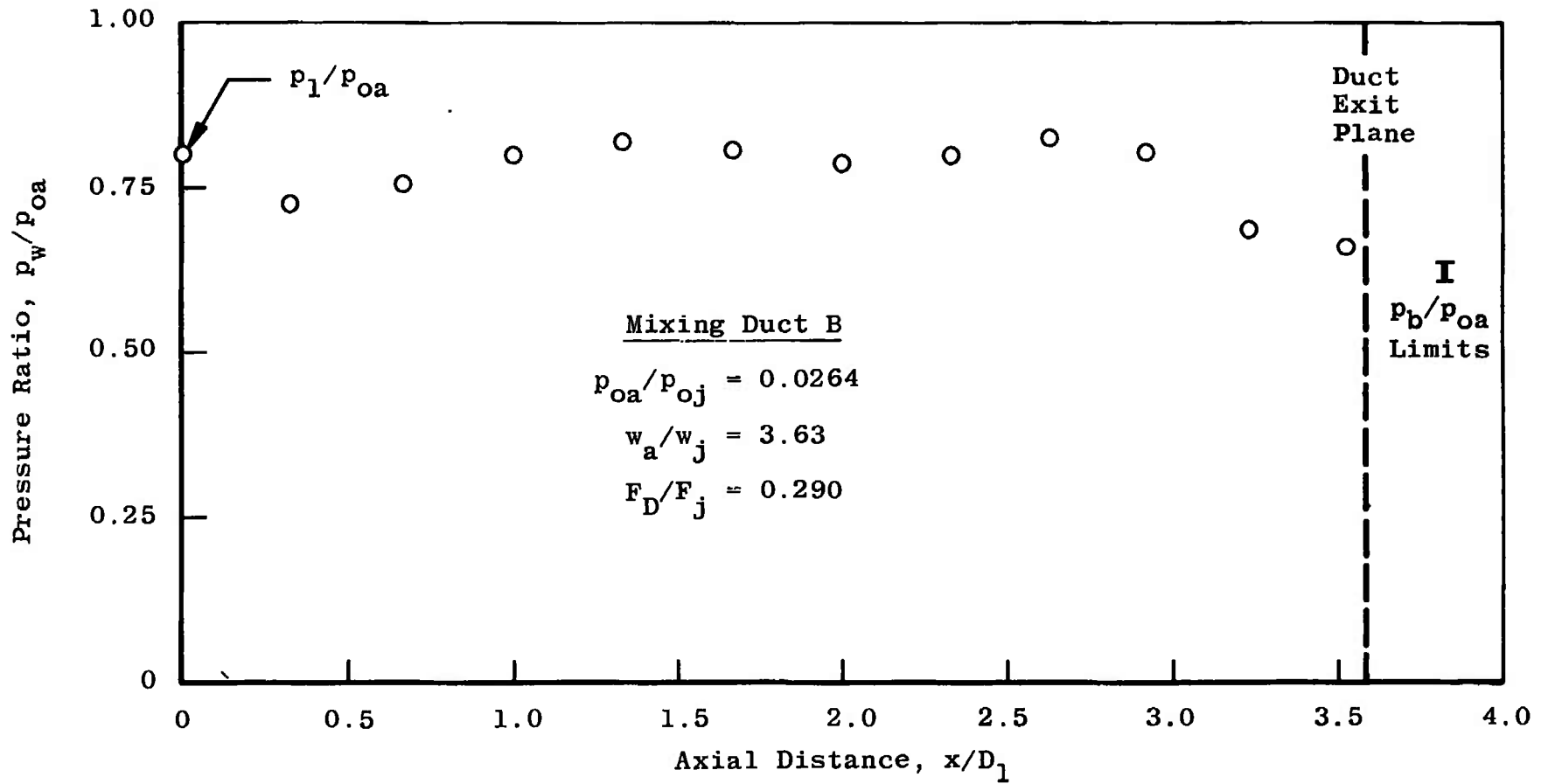
b. Test Condition 8  
 Fig. 12 Continued



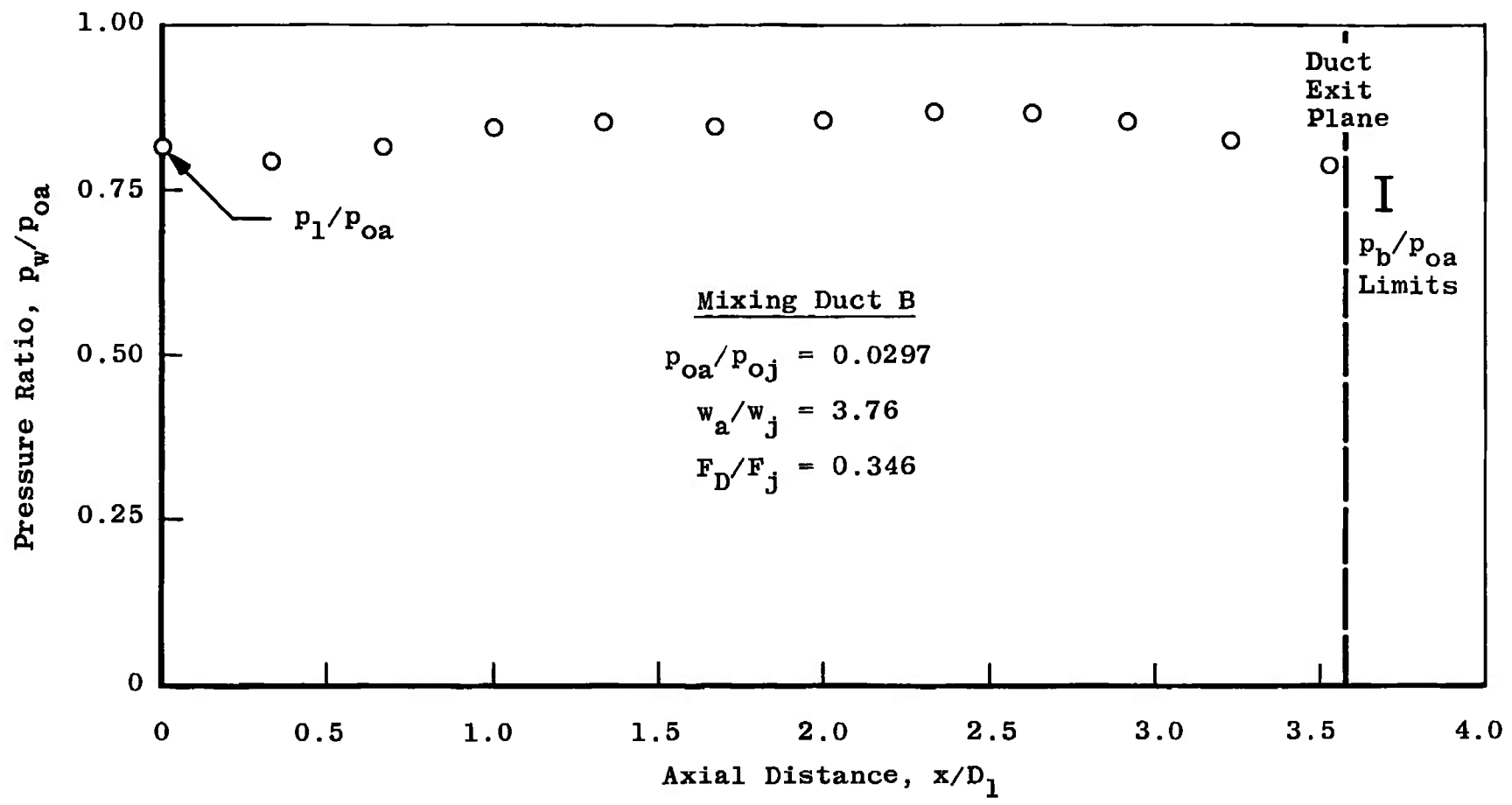
c. Test Condition 9  
 Fig. 12 Continued



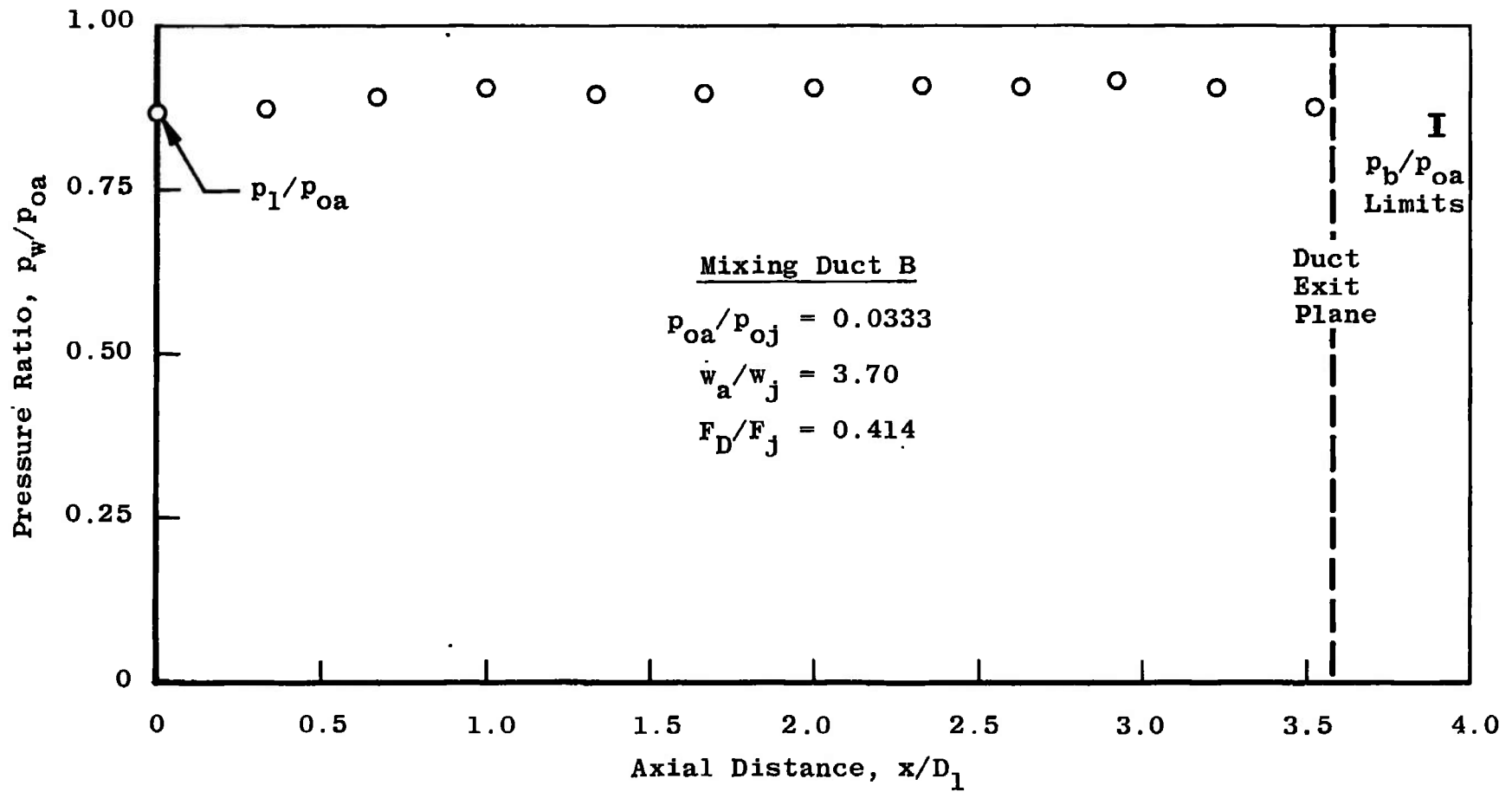
d. Test Condition 10  
 Fig. 12 Continued



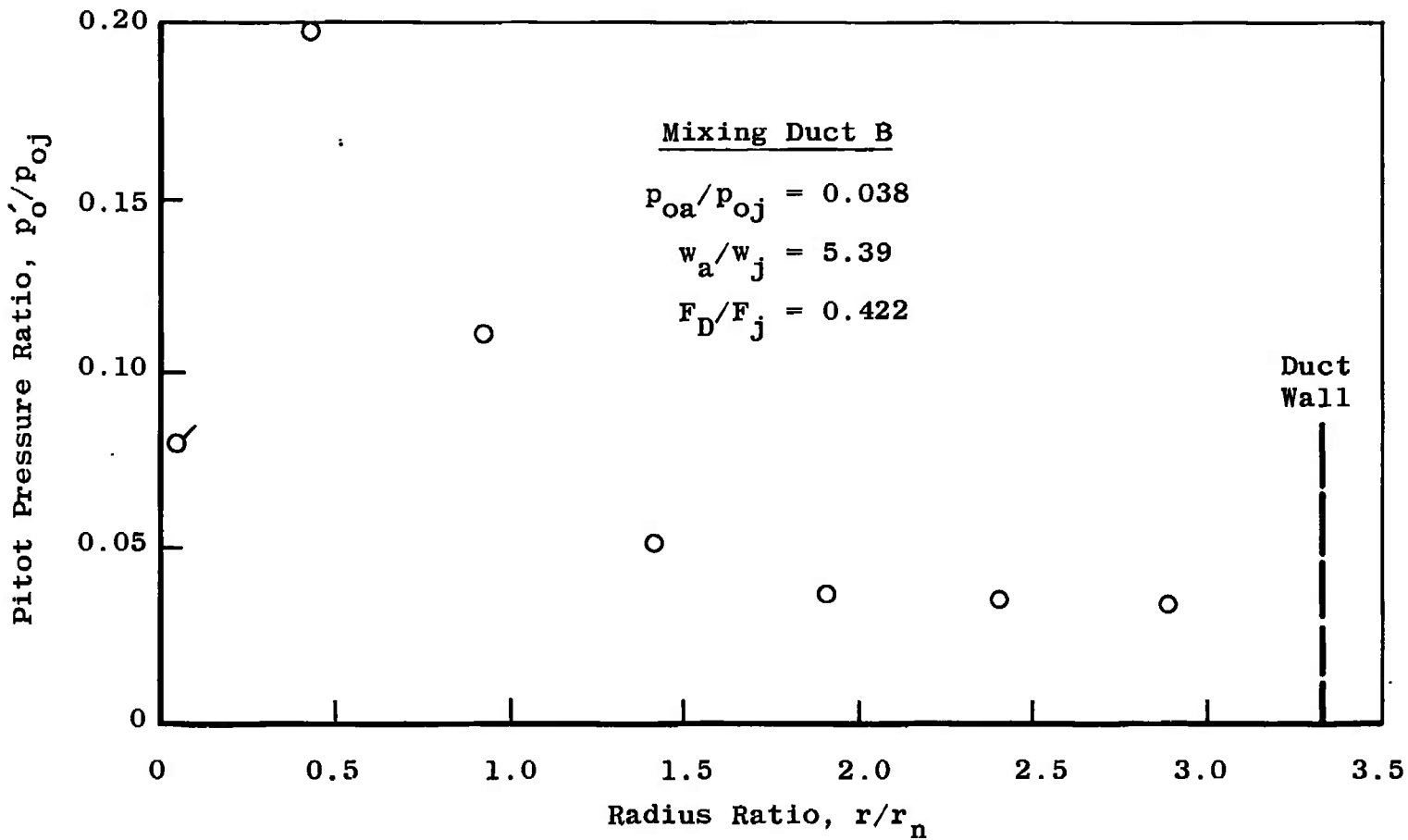
e. Test Condition 11  
 Fig. 12 Continued



f. Test Condition 12  
Fig. 12 Continued

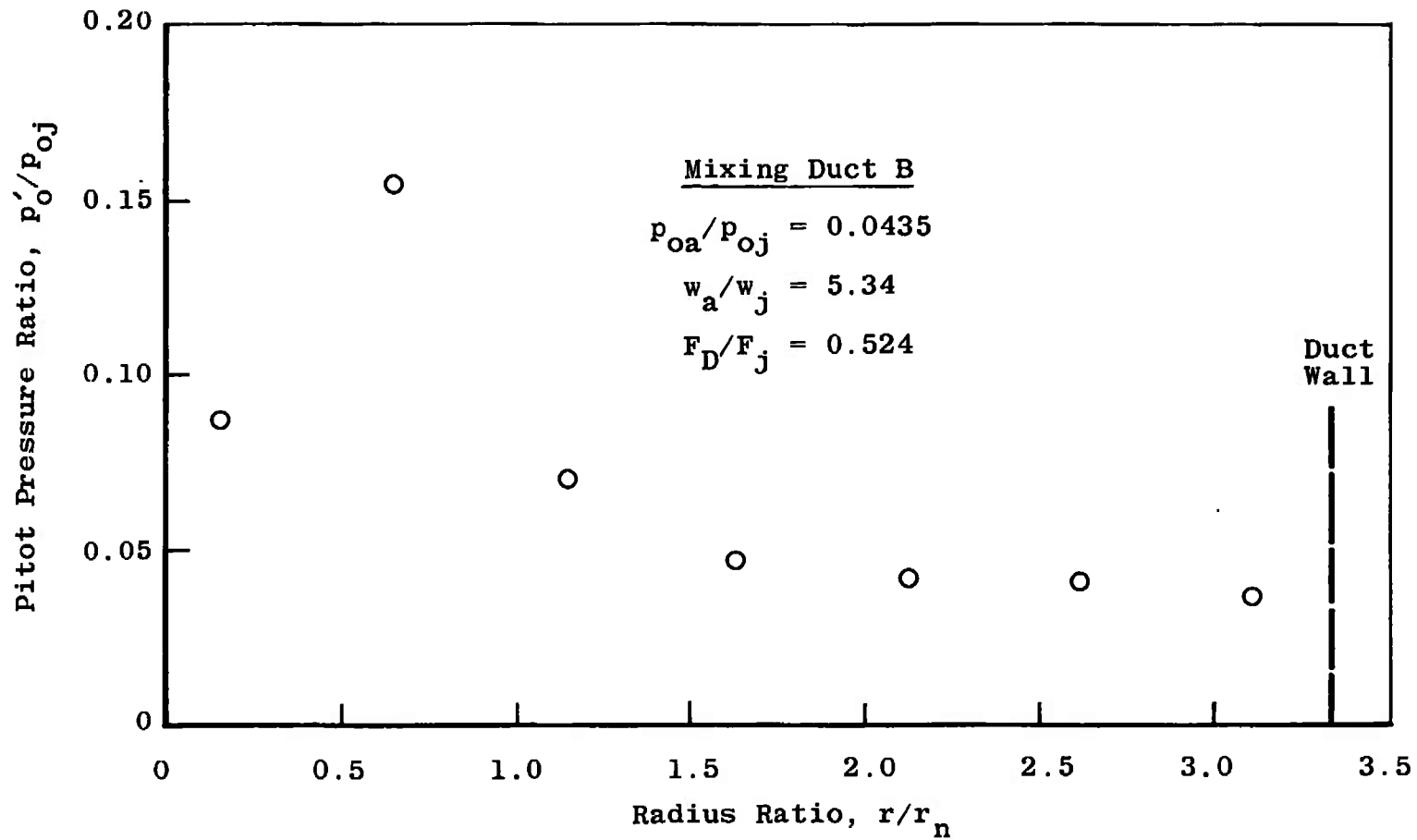


g. Test Condition 13  
Fig. 12 Concluded

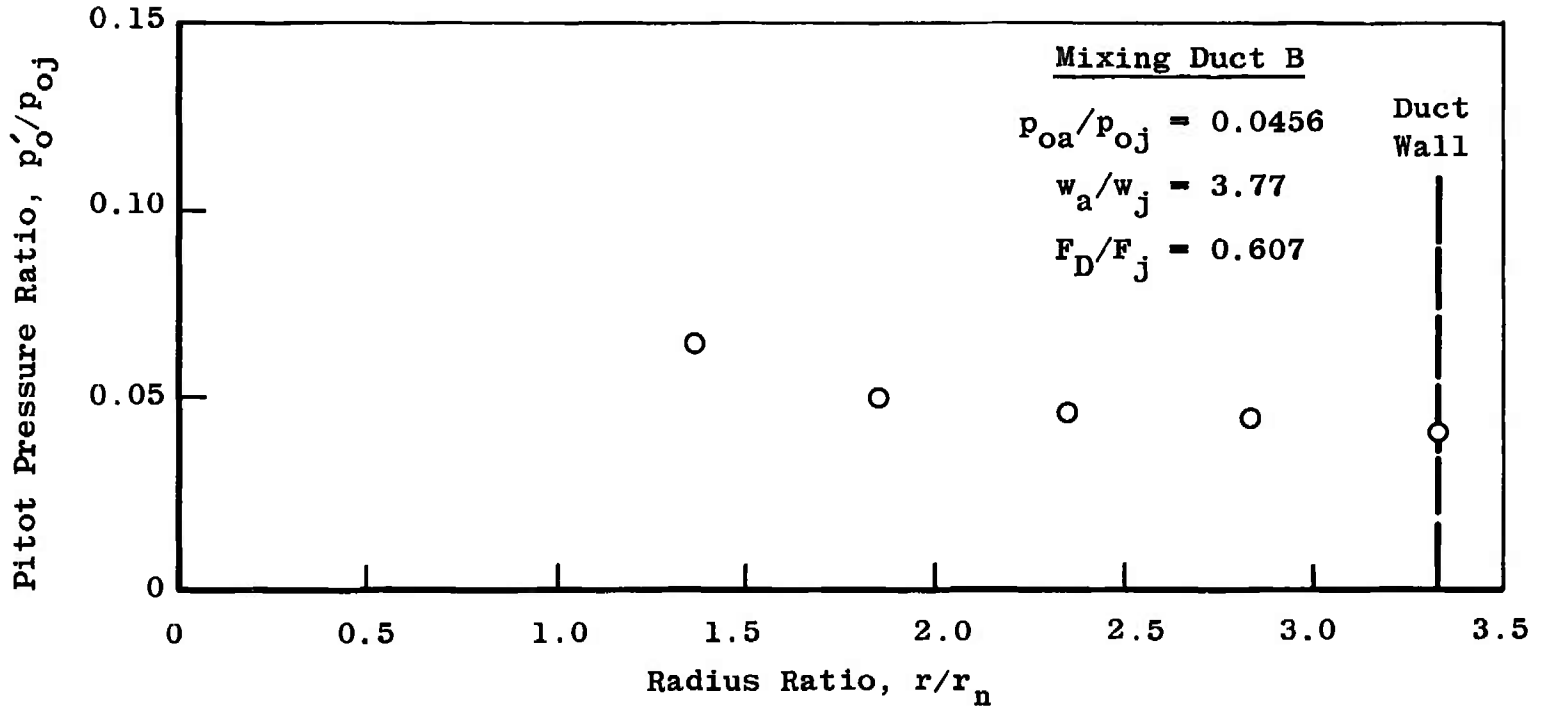


a. Test Condition 8

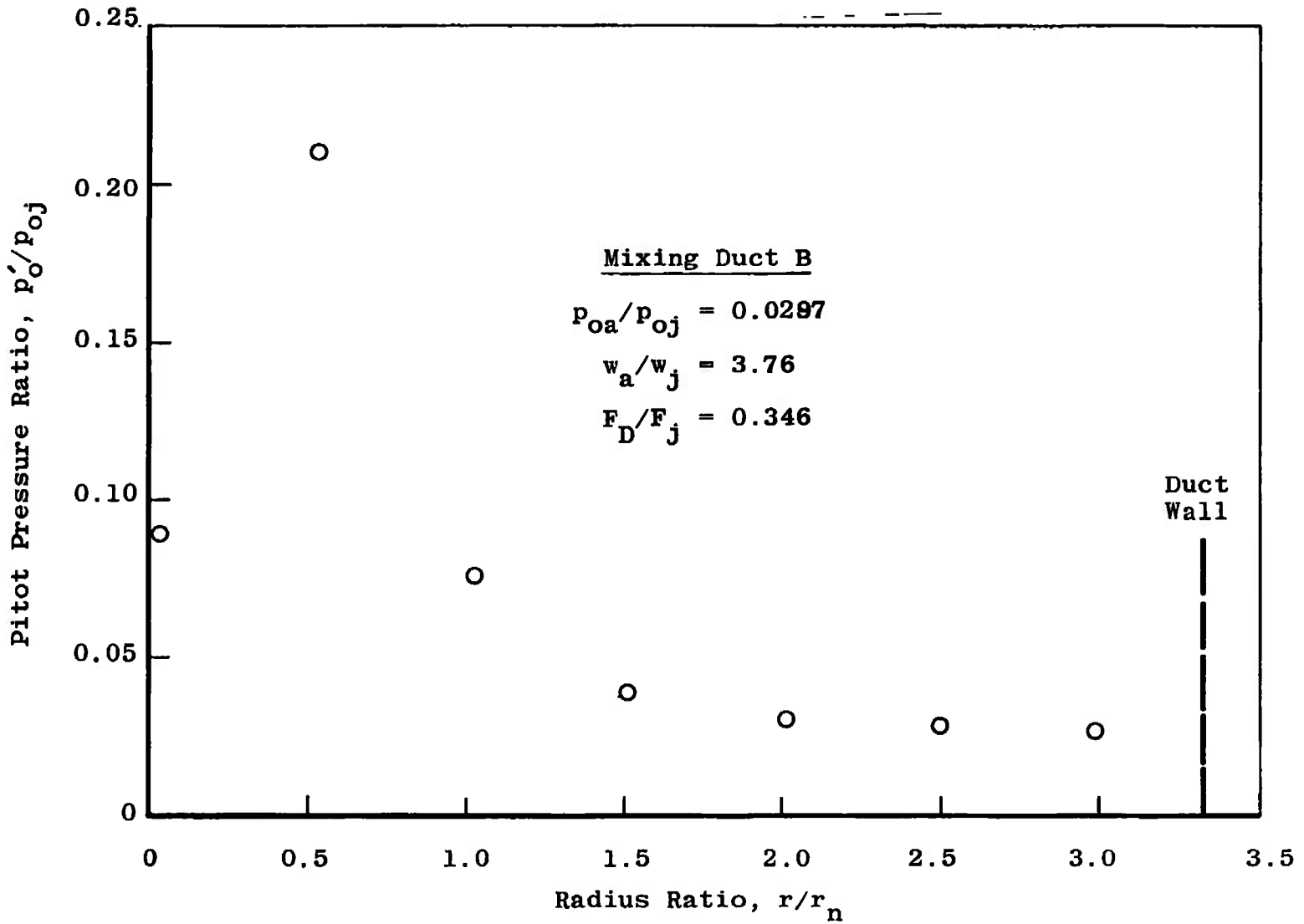
Fig. 13 Pitot Pressure at Duct Exit, Back Pressure Dependent Mode



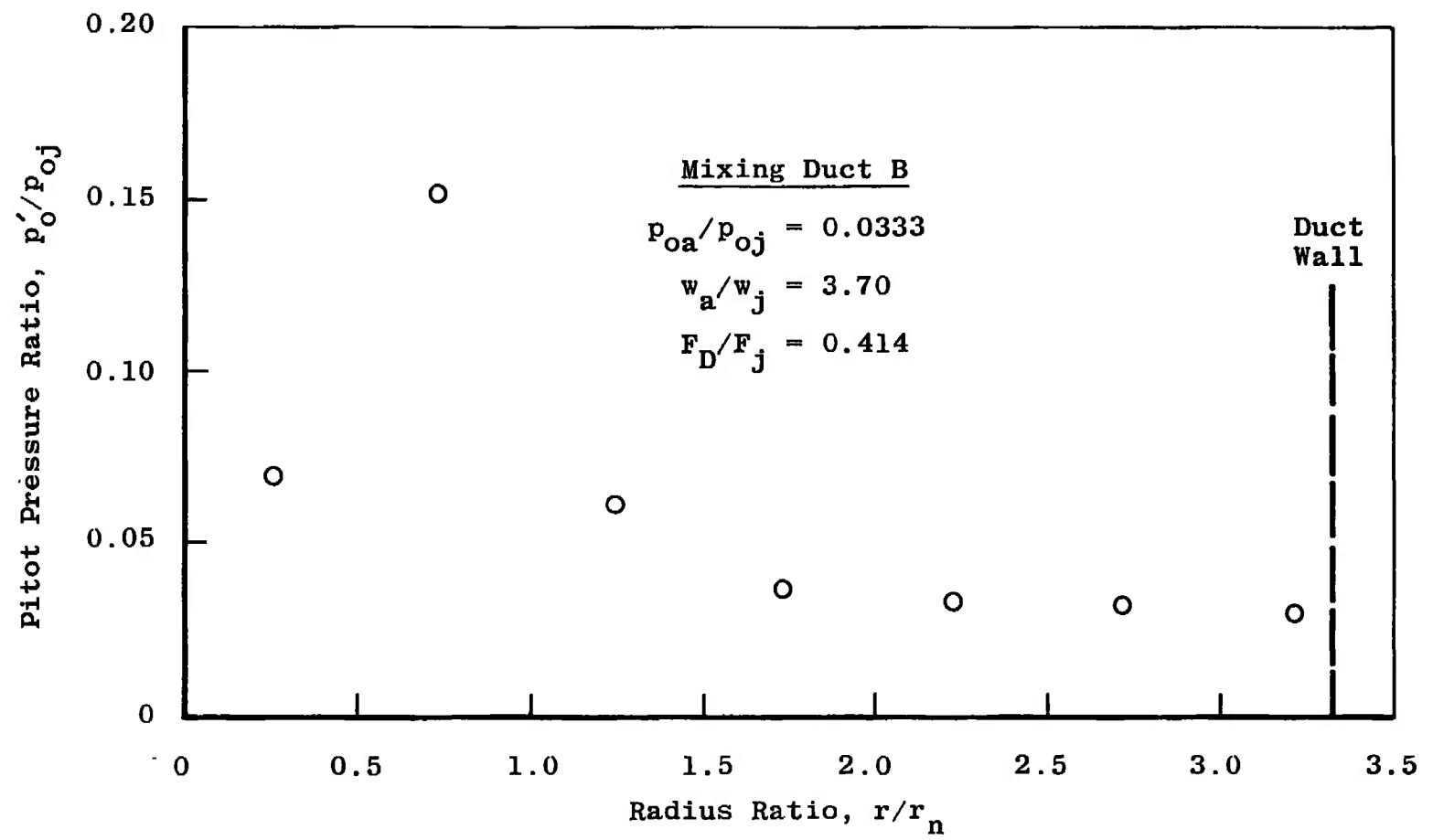
b. Test Condition 9  
Fig. 13 Continued



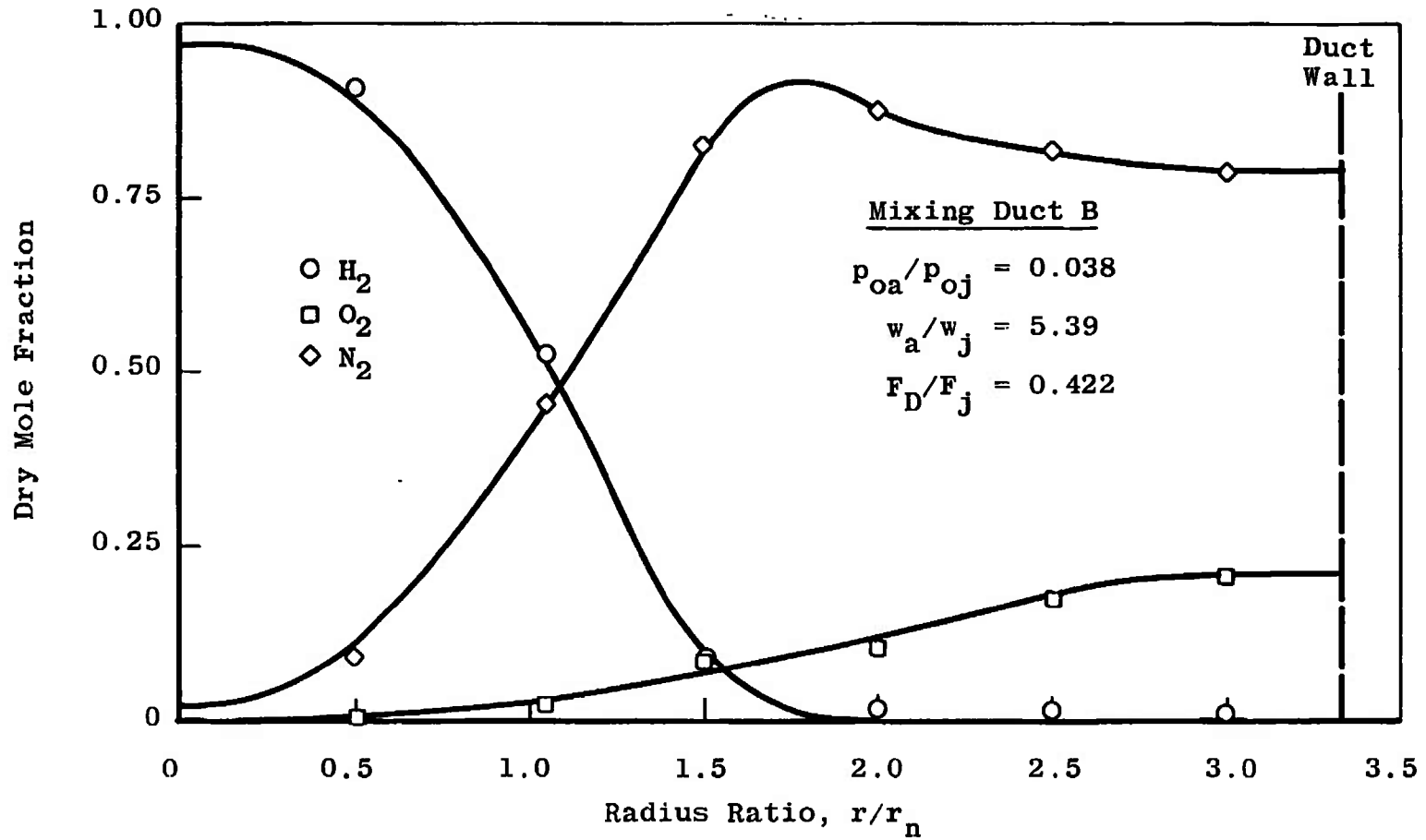
c. Test Condition 10  
 Fig. 13 Continued



d. Test Condition 12  
Fig. 13 Continued

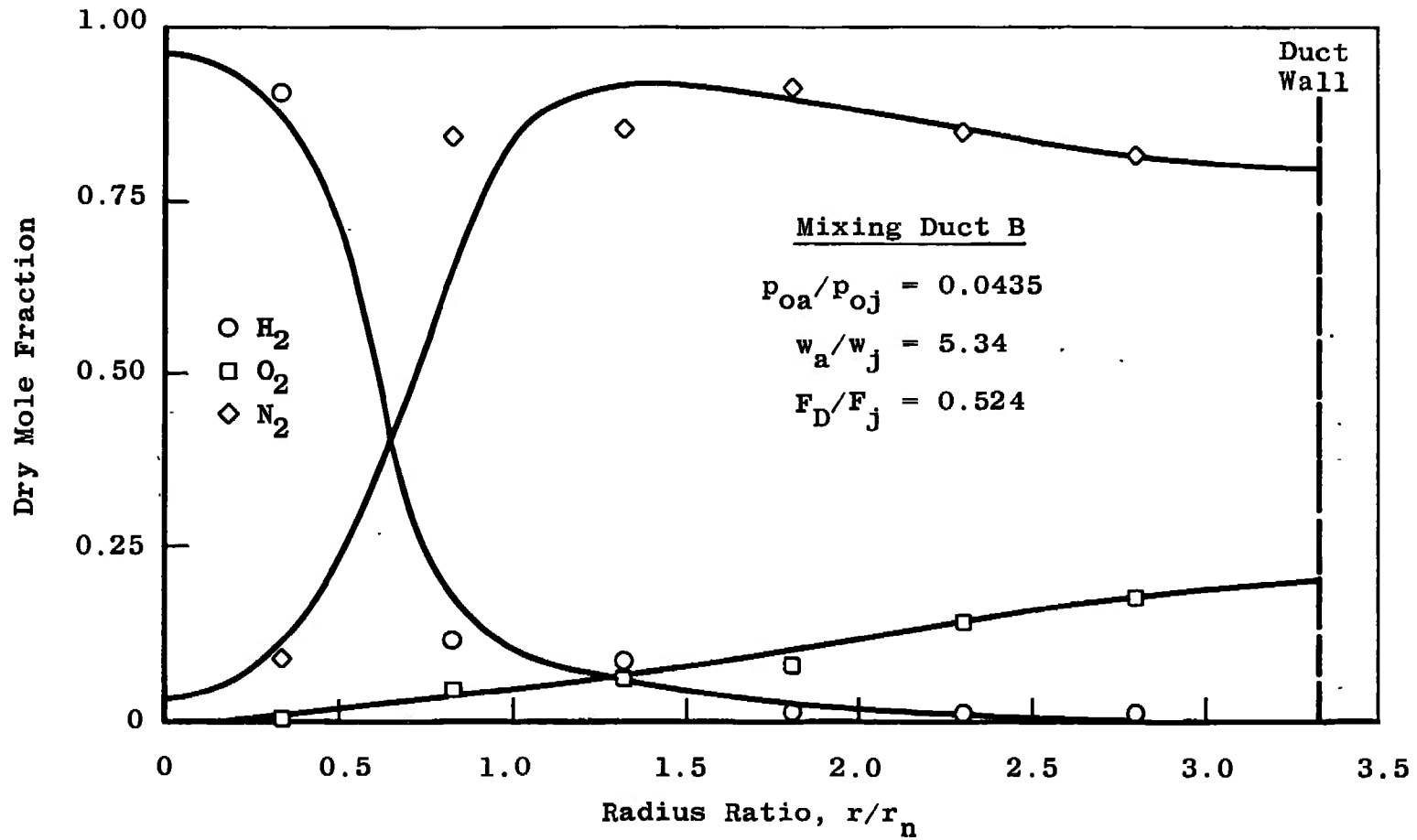


e. Test Condition 13  
Fig. 13 Concluded

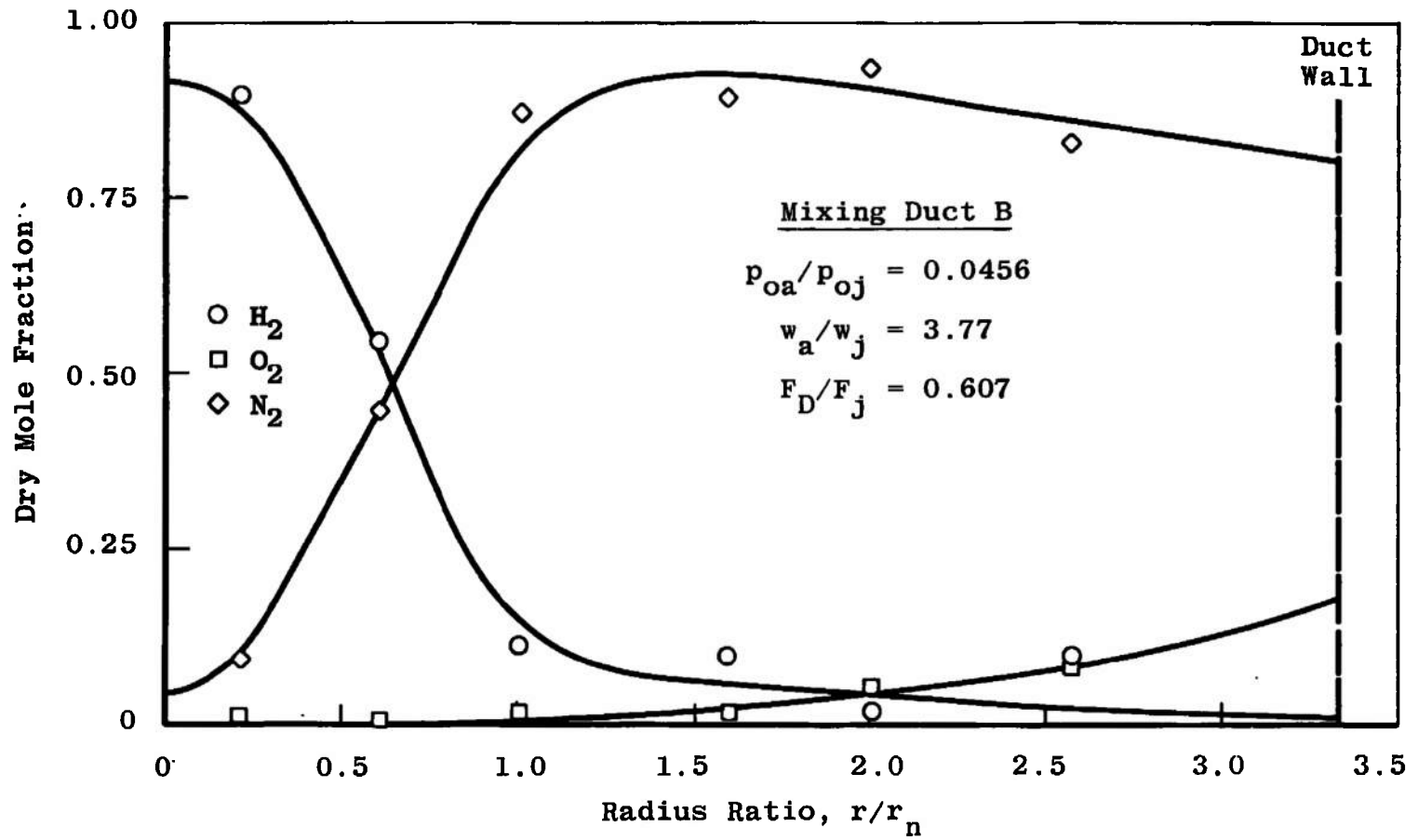


a. Test Condition 8

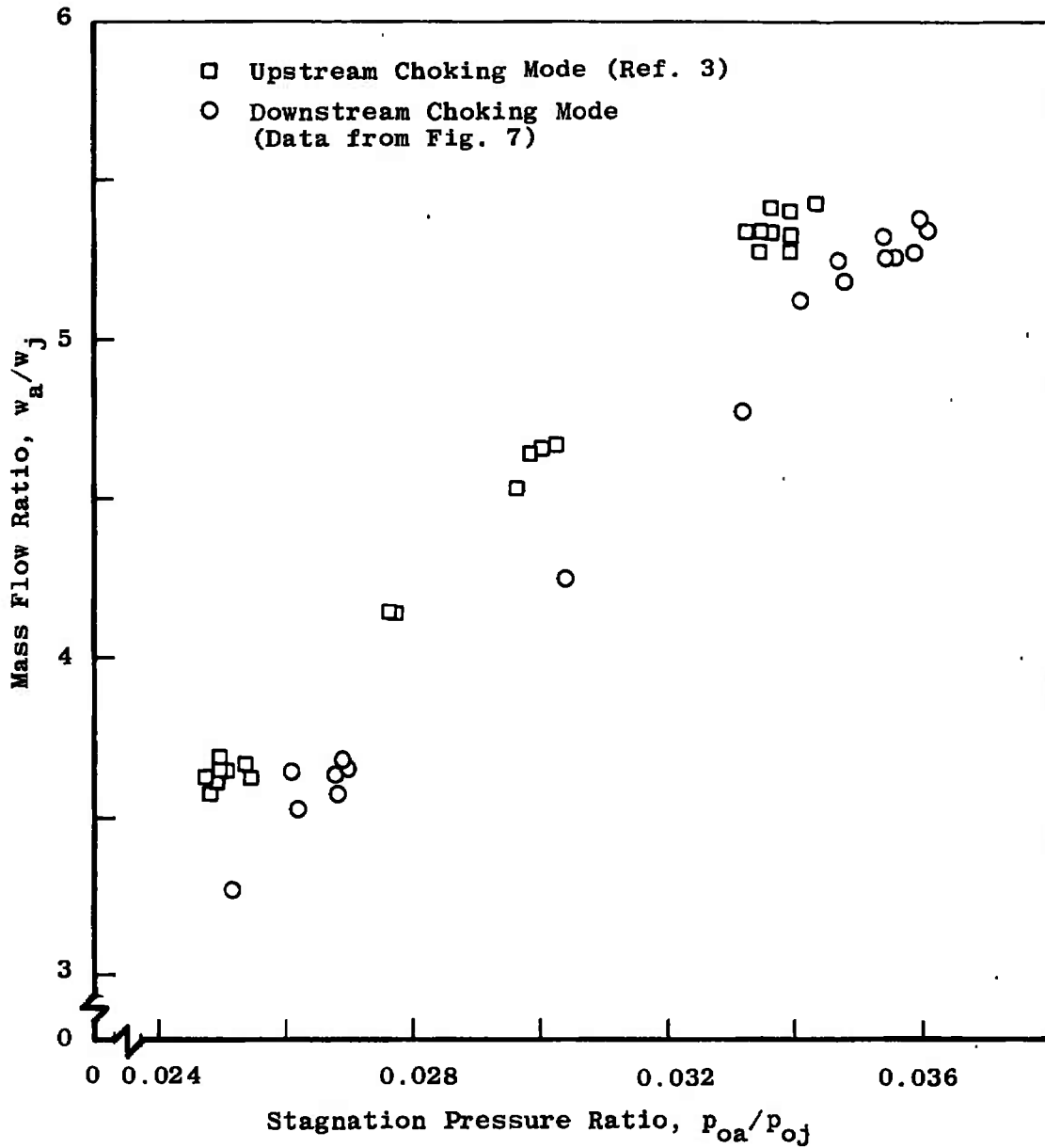
Fig. 14 Composition at Duct Exit, Downstream Choking Mode



b. Test Condition 9  
Fig. 14 Continued

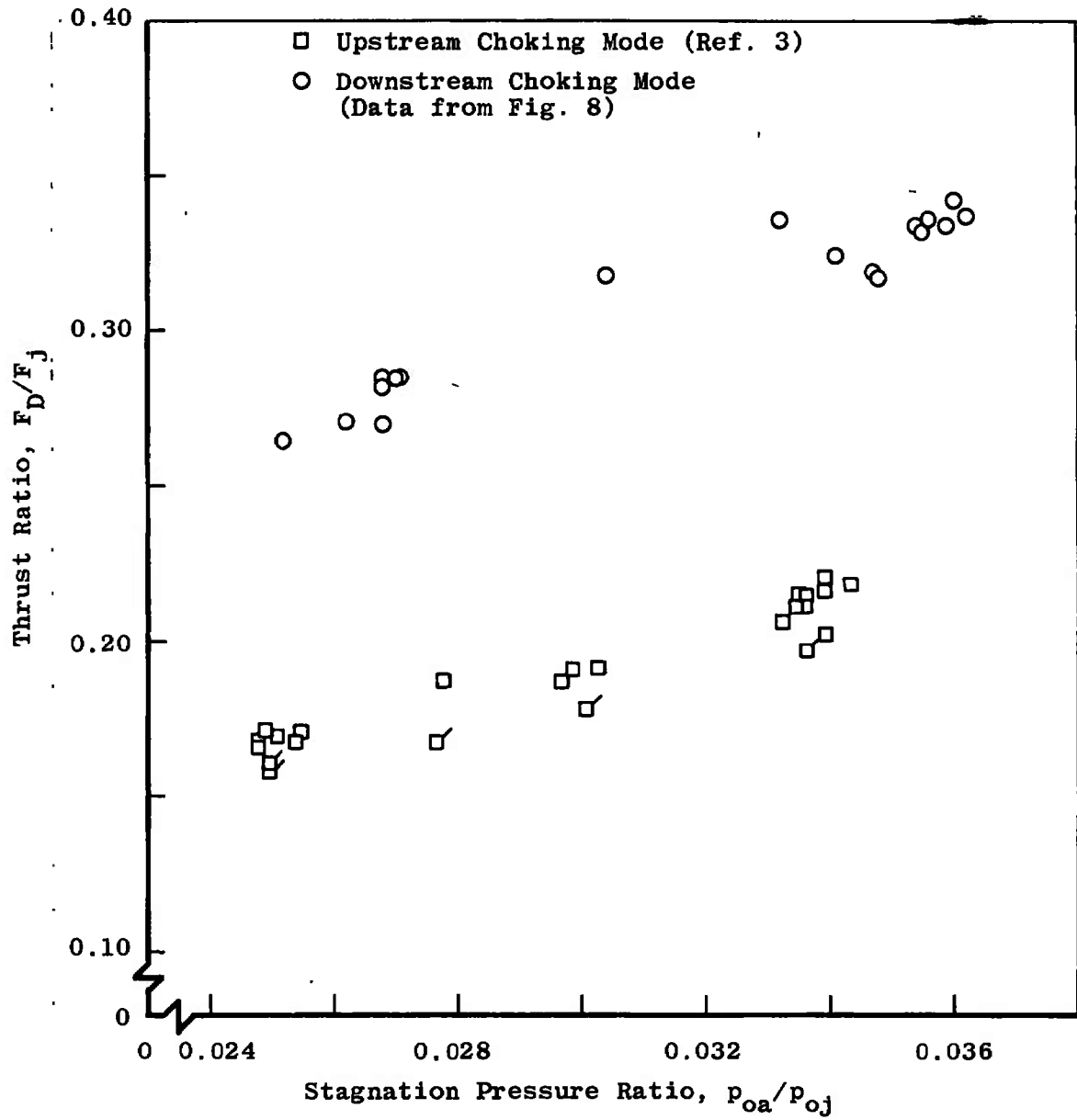


c. Test Condition 10  
 Fig. 14 Concluded



a. Mass Flow Ratio

Fig. 15 Comparison of Upstream Choking and Downstream Choking Modes



b. Thrust Ratio  
Fig. 15 Concluded

**TABLE I**  
**EXPERIMENTAL PARAMETERS**

Nominal Rocket Parameters

Oxidizer	Gaseous oxygen
Fuel	Gaseous hydrogen
Chamber pressure ( $p_{Oj}$ )	300 psia
Calculated vacuum thrust ( $F_j$ )	374 $lb_f$
Characteristic velocity ( $c^*$ )	7634 ft/sec
Mixture ratio, by mass (O/F)	3.15
Total propellant mass flow ( $w_j$ )	0.99 $lb_m/sec$
Throat diameter	1.00 in.
Nozzle exit radius ( $r_n$ )	1.143 in.
Nozzle configuration	15-deg half-angle conical

Mixing Duct

Inlet diameter ( $D_1$ )	6 in.
Length of conical section ( $L_1$ )	15.5 in.
Divergence half-angle of cone	2.98 deg
Length of cylindrical extension ( $L_2$ )	
Configuration B	6 in.
Configuration C	9 in.
Diameter of cylindrical extension ( $D_2$ )	7.6 in.
Nominal air temperature ( $T_{Oa}$ )	530°R

**TABLE II**  
**SUMMARY OF TEST CONDITIONS, DOWNSTREAM CHOKING MODE**

Test Condition	$P_{0a}/P_{0j}$	$w_a/w_j$	$F_D/F_j$	$P_{0j}$ , psia	$w_j$ , lb <sub>m</sub> /sec	O/F	$c^*$ , ft/sec	$F_D$ , lb <sub>f</sub>	$T_{0a}$ , °R	$L_2$ , in.
1	0.0433	5.36	0.510	285.3	0.962	3.16	7495	181.6	530	9
2a	0.0354	5.32	0.334	296.0	0.978	3.12	7630	123.2	525	6
2b	0.0341	5.12	0.324	310.1	1.008	3.32	7750	125.1	529	6
2c	0.0356	5.26	0.336	294.4	0.981	3.19	7563	123.9	530	6
2d	0.0355	5.26	0.332	295.7	0.985	3.22	7571	122.4	526	6
2e	0.0348	5.19	0.317	304.0	1.003	3.24	7639	120.3	523	6
2f	0.0347	5.25	0.319	302.0	0.994	3.21	7655	120.5	520	6
2g	0.0359	5.26	0.334	293.1	0.984	3.22	7511	122.2	531	6
2h	0.0362	5.35	0.337	291.1	0.968	3.13	7578	122.8	531	6
2i	0.0360	5.38	0.342	292.4	0.965	3.10	7635	124.7	528	6
2 (av)	0.0354	5.27	0.331	297.6	0.985	3.19	7615	122.8	527	6
3a	0.0268	3.60	0.285	295.4	0.981	3.12	7589	105.1	528	6
3b	0.0268	3.57	0.270	312.5	0.996	3.26	7904	105.1	531	6
3c	0.0270	3.62	0.285	295.7	0.986	3.21	7562	105.2	531	6
3d	0.0262	3.53	0.271	303.3	1.003	3.25	7623	102.7	525	6
3e	0.0271	3.63	0.285	292.1	0.974	3.18	7559	103.6	533	6
3f	0.0268	3.64	0.282	292.4	0.969	3.13	7604	102.8	532	6
3 (av)	0.0268	3.60	0.276	298.6	0.985	3.19	7640	104.1	530	6
4	0.0304	4.25	0.318	291.8	0.964	3.13	7629	115.8	534	6
5	0.0332	4.78	0.336	291.8	0.971	3.13	7570	122.2	532	6
6	0.0252	3.29	0.265	292.4	0.971	3.13	7587	96.7	533	6

TABLE III  
SUMMARY OF TEST CONDITIONS, BACK PRESSURE DEPENDENT MODE

Test Condition	$P_{0a}/P_{0j}$	$P_b/P_{0j}$	$P_D/P_{0j}$	$w_a/w_j$	$F_D/F_j$	$P_{0j}$ , psia	$w_j$ , lb <sub>m</sub> /sec	O/F	$c^*$ , ft/sec	$F_D$ , lb <sub>f</sub>	$T_{0a}$ , °R	$L_2$ , in.
7	0.0354	0.0178	0.0192	5.41	0.353	301.0	0.959	3.10	7976	133.0	532	6
8	0.0380	0.0248	0.0268	5.39	0.422	294.0	0.960	3.03	7717	154.9	530	6
9	0.0435	0.0331	0.0348	5.34	0.524	289.8	0.967	3.07	7554	189.0	531	6
10	0.0456	0.0423	0.0432	3.77	0.607	302.8	0.976	3.03	7820	228.8	531	6
11	0.0264	0.0161	0.0167	3.63	0.290	297.8	0.955	3.10	7923	108.0	532	6
12	0.0297	0.0214	0.0228	3.76	0.346	292.5	0.947	3.00	7783	126.0	530	6
13	0.0333	0.0278	0.0288	3.70	0.414	290.6	0.969	3.03	7563	149.9	531	6

## DOCUMENT CONTROL DATA - R &amp; D

(Security classification of title, body of abstract and indexing annotation must be entered when the overall report is classified)

1. ORIGINATING ACTIVITY (Corporate author) Arnold Engineering Development Center ARO, Inc., Operating Contractor Arnold Air Force Station, Tennessee		2a. REPORT SECURITY CLASSIFICATION <b>UNCLASSIFIED</b>	
		2b. GROUP N/A	
3. REPORT TITLE FURTHER EXPERIMENTS ON MIXING AND BURNING OF BOUNDED COAXIAL STREAMS			
4. DESCRIPTIVE NOTES (Type of report and inclusive dates) Final Report			
5. AUTHOR(S) (First name, middle initial, last name) T. H. M. Cunningham and C. E. Peters, ARO, Inc.			
6. REPORT DATE October 1968	7a. TOTAL NO. OF PAGES 64	7b. NO. OF REFS 7	
8a. CONTRACT OR GRANT NO. F40600-69-C-0001 b. Program Element 6540223F	9a. ORIGINATOR'S REPORT NUMBER(S) AEDC-TR-68-136		
c. d.	9b. OTHER REPORT NO(S) (Any other numbers that may be assigned this report) N/A		
10. DISTRIBUTION STATEMENT This document has been approved for public release and sale; its distribution is unlimited.			
11. SUPPLEMENTARY NOTES Available in DDC		12. SPONSORING MILITARY ACTIVITY Arnold Engineering Development Center, Air Force Systems Command, Arnold Air Force Station, Tennessee	
13. ABSTRACT Results of bounded mixing and burning experiments in relatively long ducts are presented. The series of experiments was part of a theoretical and experimental investigation of bounded mixing with combustion within ducts of arbitrary shape. The mixing system consisted of a fuel-rich, H <sub>2</sub> -O <sub>2</sub> rocket stream and a surrounding stream of room-temperature air. A conical mixing duct with cylindrical extensions was used. Twenty-six rocket firings were made in the test series. The system was operated in the "downstream choking" mode (independent of back pressure) for 19 firings and in the "back pressure dependent" mode for the remainder of the series. Stagnation pressure ratio between the two streams was varied to provide a range of data. Data presented include axial distributions of wall static pressure and radial profiles of gas composition and pitot pressure at the mixing duct exit.			

14. KEY WORDS	LINK A		LINK B		LINK C	
	ROLE	WT	ROLE	WT	ROLE	WT
rocket exhausts						
turbulent mixing						
air-augmented rockets						
jet mixing						
ducts						
pressure distribution						
hydrogen-oxygen mixtures						
3. Coaxial streams						
4 " "						

3. Coaxial streams -- Mixing

4 " " -- ~~Burn~~  
Combustion

10-5.